UCLA
COMPUTATIONAL AND APPLIED MATHEMATICS

Efficient Implementation of Essentially Non-Oscillatory Schemes for Systems of Nonlinear Hyperbolic Differential Equations

Edgard Katzer
Stanley Osher

May 1988

CAM Report 88-14

Department of Mathematics
University of California, Los Angeles
Los Angeles, CA. 90024-1555

Efficient Implementation of Essentially Non-Oscillatory Schemes for Systems of Nonlinear Hyperbolic Differential Equations.

Edgar KATZER and Stanley OSHER*

Department of Mathematics

University of California at Los Angeles

ABSTRACT

Efficient implementations of of the Runge-Kutta type essentially non-oscillatory (ENO) scheme of Shu and Osher [1] for nonlinear strictly hyperbolic systems of conservation laws are presented. These new schemes are applied to numerical test problems of one-dimensional gas dynamics and the results are compared with results of the MacCormack scheme [2] and the total variation diminishing (TVD) scheme of Davis [3]. The interaction of a shock with an entropy wave is used as a crucial test for the numerical algorithms. The results of the ENO schemes are more acurate then those of the TVD scheme and are more reliable than those of the MacCormack scheme. The new schemes avoid a field by field decomposition of the flux and are much faster than the original version.

May 2, 1988

* present address: Institute of Informatics and Applied Mathematics, Christian Albrecht University, 2300 K I E L, West Germany.

It is gratefully acknowledged that research for the first author has been made possible by the hospitality of the Department of Mathematics at UCLA and by financial support of the Deutsche Forschungsgemeinschaft (German Science Foundation) under contract number Ka 742/1-1.

Efficient Implementation of Essentially Non-Oscillatory Schemes for Systems of Nonlinear Hyperbolic Differential Equations.

Edgar KATZER and Stanley OSHER*

Department of Mathematics

University of California at Los Angeles

1. Introduction

We present efficient essentially non-oscillatory numerical schemes for solving nonlinear hyperbolic systems of conservation laws in one space dimension. Consider the initial value problem:

$$\begin{aligned} u_t + f(u)_x &= 0 \\ u(x,0) &= u^0(x) \\ u, f(u) &: \mathbf{R}^2 \to \mathbf{R}^d \end{aligned} \tag{1.1}$$

This system is assumed to be strictly hyperbolic, i. e. the Jacobian:

$$A = \frac{\partial f}{\partial u} \tag{1.2}$$

has a complete set of eigenvalues and left and right eigenvectors. In the applications we always consider the case of one-dimensional gas dynamics (Owczarek [4]). Here

* present address: Institute of Informatics and Applied Mathematics, Christian Albrecht University, 2300 K I E L, West Germany.
It is gratefully acknowledged that research for the first author has been made possible by the hospitality of the Department of Mathematics at UCLA and by financial support of the Deutsche Forschungsgemeinschaft (German Science Foundation) under contract number Ka 742/1-1.

the vector of density, momentum and total energy and the flux f is given by:

$$\begin{aligned} u &= (\rho\ ,\ \rho v\ ,\ \rho\varepsilon) \\ f &= (\rho v\ ,\ \rho v^2+p\ ,\ (\rho\varepsilon+p)v\ ) \end{aligned} \tag{1.3}$$

where $p = (\gamma-1)\rho(\varepsilon-\frac{1}{2}v^2)$ is the pressure ($\gamma = 1.4$).

It is well known (Lax [5]) that weak solutions of (1.1) may have discontinuities or discontinuous derivatives. These discontinuities correspond to shock waves, contact discontinuities and the head and tail of expansion fans. Many 'classical' numerical methods for solving (1.1) either are only first order accurate or produce numerical oscillations near these discontinuities. See Sod [6] for a discussion and comparison of various schemes. Total variation diminishing (TVD) schemes, a concept introduced by Harten [7], avoid these oscillations, but they degenerate to first order accuracy near extrema of the solution. For a classification of these schemes see Sweby [8] and Jameson and Lax [9] and the literature there. Osher and Chakravarty [10] presented TVD schemes up to order fifteen.

Recently Harten and Osher [11] and Harten et al. [12], [13] have developed so called essentially non-oscillatory schemes (ENO schemes). These are almost free of numerical oscillations, and remain of uniformly high order of accuracy in smooth regions of the flow and up to the shock. Shu and Osher [1], [14] derived more economic ENO schemes which avoid the reconstruction of the solution from their averages. They are based on the flux values only, and apply a TVD Runge-Kutta procedure for the time discretisation.

Basic principle of the ENO schemes is the usage of an adaptive stencil depending on the smoothness of the numerical data for reconstructing the solution or the flux. This adaptive stencil automatically chooses the data corresponding to the least oscillating plynomial, and leads to an highly nonlinear scheme even in the case of a linear equation with constant coefficients. See Osher and Sweby [15] for a short review.

Clearly ENO schemes are more expensive than linear schemes, as for example the MacCormack scheme [2]. But they are worth it if one is interested in accurate solutions without numerical oscillations which are designed to simulate a physical mechanism correctly. This is of particular importance if the physical problem to be simulated numerically contains much internal structure. In Chapter 2 we present a test problem which is a simplified model of shock/turbulence interaction. The numerical results in chapter 4 for that test problem clearly show that ENO schemes are superior to the MacCormack scheme and the TVD scheme of Davis [3].

The extension of the ENO schemes to nonlinear systems further increases the numerical effort. This is due to the fact, that this extension is based on a field by field decomposition of the flux. This requires the calculation of the eigenvectors and several matrix multiplications at each grid point. In chapter 3 we present several more efficient implementations of ENO schemes for nonlinear systems, which reduce the numerical work greatly. These schemes avoid expensive eigenvalue decompositions and matrix multiplications at the cost of a slightly reduced accuracy. In chapter 4 we compare the numerical results for these new schemes with the field by field decomposition scheme, the MacCormack scheme [2] and the TVD scheme of Davis [3].

2. A One-Dimensional Model of Shock/Turbulence Interaction — A Numerical Test Problem.

Riemann problems proposed by Sod [6] and Lax [5] have been commonly used as test problems for comparison of numerical algorithms designed to calculate compressible flows. These test problems are well suited to demonstrate the capability of an algorithm to capture discontinuities. But in smooth regions the exact solution of a Riemann problem either is constant or may be sufficiently approximated by a linear function. A Riemann problem has a very simple structure and these test cases are no challenging problem in smooth regions.

In engineering applications, numerical schemes are supposed to be applied to the calculation of complicated flows around aircraft and reentry vehicles, and in combustion engines. There are regions with higly complex internal structure embedded in these flowfields. (See Katzer, Reister and Oertel [16],[17],[18] for examples of such structures.) The interaction of a shock with a turbulent flow is one of the challenging problems of fluid mechanics. It is an highly nonlinear, three-dimesional unsteady phenomenon, which is not understood in detail. See Delery and Marvin [19] for a review and Zang et al. [20], for numerical and Haas and Sturtevant [21] and Hesselink and Sturtevant [22] for experimental results. This phenomenon inspired a simplified model of shock/turbulence interacion which is simple enough to serve as a test problem but posesses more structure than a Riemann problem.

Consider the one-dimensional problem of a shock traveling into a nonhomogeneous flow region. The initial conditions are:

$$\begin{array}{ll} \rho^0(x) = \rho_2 & \text{if } x \le 0 \\ \rho^0(x) = \rho_1 - \rho_{11}\sin(\kappa x) & \text{if } x > 0 \\ p^0(x) = p_2 & \text{if } x \le 0 \\ p^0(x) = p_1 & \text{if } x > 0 \\ v^0(x) = v_2 & \text{if } x \le 0 \\ v^0(x) = v_1 & \text{if } x > 0 \end{array} \tag{2.1}$$

The jumps:

$$\begin{array}{l} \rho_2 - \rho_1 \\ p_2 - p_1 \\ v_2 - v_1 \end{array} \tag{2.2}$$

fulfill the Rankine-Hugoniot conditions for a given shock speed v_{sh}. Here ρ_{11} is the amplitude and κ the wave number of a density wave impinging the shock. The density wave is a model (admittedly very crude) of turbulent flow ahead of the shock. Notice that we obtain a Riemann problem whose solution is given by a simple shock if ρ_{11} vanishes. Problem (2.1) is a distorted Riemann problem.

Let us first discuss what kind of solution we would expect for small amplitudes (small compared to the shock strength $\rho_2 - \rho_1$ and the mean density ahead of the shock ρ_1). Then we have a small disturbance of a running shock. Acoustic theory is valid ahead of and behind the shock, and we may linearize the Rankine-Hugoniot equations which couple the solutions on both sides of the shock. Details can be found in McKenzie and Westphal [23]. We consider the solution in a coordinate system which moves with the shock (figure 1). The density wave may be considered as an entropy wave impinging on the shock. The interaction with the shock generates three waves behind the shock:

- a fast acoustic wave running with speed v_2+c_2.

  This wave immediately merges with the shock thereby changing its strength and speed.

- a slow acoustic wave running with speed v_2-c_2 and
- a transmitted entropy wave running with speed v_2.

Here c_2 is the sound speed in the region behind the shock. We expect no reflected wave ahead of the shock because the shock runs faster than the fast acoustic wave in the region ahead of the shock. Thus we have a clean entropy wave impinging on the shock.

For larger amplitudes we expect the same type of wave pattern. But now the the waves behind the shock interact with each other nonlinearly, and the acoustic waves would steepen and eventually generate left running shocks. This global picture is valid as long as the density waves ahead of the shock are not too large. For very large amplitudes the variation of the sound speed in the region ahead of the shock is larger than the shock speed. This weakens the the shock periodically so that the shock degenerates to a fast acoustic wave.

3. Essentially Non-Oscillatory Schemes

We first recall the Runge-Kutta type essentially non-oscillatory schemes with Lax-Friedrichs building block introduced by Shu and Osher [1]. In chapter (3.2) we extend these schemes to linear, and in chapter (3.3) to nonlinear, systems. In (3.4) we introduce simplifications which reduce the numerical work involved with the field by field decomposition and avoid the calculation of the eigenvectors. For the case of the one-dimensional gas dynamic equations a further simplification is presented.

3.1 Runge-Kutta Type Essentially Non-Oscillatory Schemes

Here we consider the scalar version ($d = 1$) of the conservation law (1.1). As usual we introduce a space and time discretisation:

$$\begin{aligned} x_j &= j\ \Delta x \\ t^n &= n\ \Delta t \end{aligned} \tag{3.1}$$

with ratio of the step sizes:

$$\lambda = \frac{\Delta t}{\Delta x} \tag{3.2}$$

and introduce grid functions:

$$\begin{aligned} u_j^n &= u(x_j, t^n) \\ f_j^n &= f(u_j^n). \end{aligned} \tag{3.3}$$

We only consider conservative discretisations:

$$u^{n+1} = u^n - \lambda(\hat{f}_{j+½} - \hat{f}_{j-½}) \tag{3.4}$$

where $\hat{f}_{j+½}$ is a consistent numerical flux between cell j and $j+1$ and depends on the grid function u_k^n near x_j and x_{j+1} .

Runge-Kutta type schemes are based on a semidiscrete method of lines approach. This allows a decoupling of the space and time discretisation. Let us first consider the

time marching procedure. We assume that we already know a numerical space operator S which approximates the flux derivatives with r^{th} order:

$$S(u) = \Delta x\, f(u)_x + O(\Delta x^{r+1}). \tag{3.5}$$

This allows the construction of a first order (in time) scheme:

$$u^{n+1} = u^n - \lambda\, S(u^n) \tag{3.6}$$

Shu and Osher [1] presented new Runge-Kutta time stepping algorithms which give higher order TVD or TV-Bounded schemes provided that the underlying first order scheme (3.6) is TVD or TV-Bounded. Here we will only recall their schemes and refer to [1] for details. We define a sequence of intermediate solutions:

$$u^{n+1} = u^{(k)}, u^{(k-1)}, \ldots, u^{(1)}, u^{(0)} = u^n \tag{3.7}$$

and define the following schemes:

1 Forward Euler method (first order scheme):

$$u^{n+1} = u^{(1)} = u^{(0)} - \lambda\, S(u^{(0)}) \tag{3.8}$$

2 Heun's predictor-corrector method (second order scheme):

$$\begin{aligned} u^{(1)} &= u^{(0)} - \lambda\, S(u^{(0)}) \\ u^{(2)} &= u^{(1)} - \lambda\, S(u^{(1)}) \\ u^{n+1} &= \tfrac{1}{2}\,(u^{(0)} + u^{(2)}) \end{aligned} \tag{3.9}$$

3 A new third order Runge-Kutta scheme:

$$\begin{aligned} u^{(1)} &= u^{(0)} - \lambda\, S(u^{(0)}) \\ u^{(2)} &= u^{(0)} - \frac{\lambda}{4}\,(S(u^{(0)}) + S(u^{(1)})) \\ u^{n+1} &= u^{(0)} - \frac{\lambda}{6}\,(S(u^{(0)}) + 4\, S(u^{(2)}) + S(u^{(1)})) \end{aligned} \tag{3.10}$$

Notice that this scheme is *not* one of the classical Runge-Kutta schemes. (The superscripts in the last equation are indeed correct.)

A reformulation of the last scheme allows a hierarchical increase of the order of accuracy, by starting with the Euler method and continuing with the Heun method to obtain the third order scheme (3.10) as:

$$\begin{aligned} u^{(3)} &= \tfrac{1}{2}\,(u^{(0)} + u^{(2)}) \\ u^{(4)} &= \tfrac{1}{2}\,(u^{(0)} + u^{(3)}) \\ u^{(5)} &= u^{(0)} - \lambda\, S(u^{(4)}) \\ u^{n+1} &= (u^{(3)} + 2u^{(5)})/3 \end{aligned} \tag{3.11}$$

These schemes (3.8) - (3.11) are stable under a CFL restriction of:

$$\lambda\, |a| \le 1.0 \tag{3.12}$$

if the basic scheme (3.6) is stabel under the same condition. We will not consider fourth and fifth order schemes provided by Shu and Osher [1] because these schemes are more complicated and possess lower CFL restrictions.

Notice that the MacCormack scheme [2] may be formulated as a Heun type method where the spatial operator in the first step is based on forward flux differences and in the second step on backward flux differences.

We now construct a non-oscillatory spatial operator S based on the local Lax-Friedrichs flux. Let:

$$\frac{1}{\lambda} \ge \alpha \ge a = \frac{\partial f}{\partial u} \tag{3.13}$$

and define:

$$\begin{aligned} f^{+} &= \tfrac{1}{2}(f + \alpha u) \\ f^{-} &= \tfrac{1}{2}(f - \alpha u) \end{aligned} \tag{3.14}$$

We obtain a decomposition of the flux into a part f^{+} with non-negative signal speed

and a part f^- with non-positive signal speed. The flux at the cell inteface between j and j+1 is then given by:

$$f_{j+½} = f^+_{j+½} + f^-_{j+½} \tag{3.15}$$

A first order upwind biased approximation of the flux is given by:

$$\begin{aligned} \hat{f}^+_{j+½} &= f_j \\ \hat{f}^-_{j+½} &= f_{j+1} \end{aligned} \tag{3.16}$$

which, in the scalar constant coefficient case, is an upwind scheme if $\alpha = a$ and the Lax-Friedrichs scheme if $\alpha = 1/\lambda$.

A Taylor series analysis shows that we obtain a $2m$ order approximation of the spatial operator S if the numerical flux fulfills:

$$\hat{f}_{j+½} = f_{j+½} + \sum_{k=1}^{m-1} \alpha_k (\Delta x)^2 \left[\frac{\partial \partial f}{(\partial x)^2} \right]_{(x_{j+½})} + O((\Delta x)^{2m+1}) \tag{3.17}$$

We require that equation (3.17) is fulfilled by the positive and negative fluxes f^+ and f^- separately. We approximate f^+ and its derivatives in the intervall $[x_j, x_{j+1}]$ by the Newton interpolation polynomial p^+ through r+1 nodes where r is the order of the spatial operator. According to the ENO adaptive stencil idea, these nodes are chosen such that the interpolant has the lowest variation and is upwind biased.

Let us first consider the numerical approxinmation of $\hat{f}^+_{j+½}$. We start with one node:

$$k^{(1)}_{\min} = k^{(1)}_{\max} = j \tag{3.18}$$

If n-1 nodes are already defined, we choose the next from the two neigbouring nodes:

$$a = k^{(n-1)}_{\min} - 1 \ , \ \ b = k^{(n-1)}_{\max} + 1 \tag{3.19}$$

such that the interpolation polynomial trough $r+1$ nodes has the smallest leading coefficient. Calculate the divided differences (Hildebrand [24]):

$$\begin{aligned} c &= f^+ \ [x_a \ , x_k \ | \ k_{\min}^{(n-1)} \le k \le k_{\max}^{(n-1)} \ ] \\ d &= f^+ \ [x_k \ | \ k_{\min}^{(n-1)} \le k \le k_{\max}^{(n-1)}, \ , x_b \ ] \end{aligned} \tag{3.20}$$

and chose:

$$\begin{aligned} k_{\min}^{(n)} &= a \ , \ k_{\max}^{(n)} = k_{\max}^{(n-1)} \qquad \text{if} \quad |c| \le |d| \\ k_{\max}^{(n)} &= b \ , \ k_{\min}^{(n)} = k_{\min}^{(n-1)} \qquad \text{if} \quad |c| > |d| \end{aligned} \tag{3.21}$$

Then p^+ is given by the Newton interpolation polynomial trough the nodes:

$$[\ x_k \ | \ k_{\min}^{(r+1)} \le k \le k_{\max}^{(r+1)}] \tag{3.22}$$

The numerical flux $\hat{f}_{j+\frac{1}{2}}^+$ is then approximated by this polynomial and its derivatives according to equation (3.17). We will denote the spatial r^{th} order adaptive stencil ENO operator by:

$$\hat{f}_{j+\frac{1}{2}}^+ = N_{j+\frac{1}{2}}^+ \ (f_k^+) \ , \quad k_{\min}^{(r+1)} \le k \le k_{\max}^{(r+1)} \tag{3.23}$$

The negative flux $\hat{f}_{j+\frac{1}{2}}^-$ is approximated in the same manner but with starting node $j+1$. The numerical flux between j and $j+1$ is then:

$$\hat{f}_{j+\frac{1}{2}} = \hat{f}_{j+\frac{1}{2}}^+ + \hat{f}_{j+\frac{1}{2}}^- \tag{3.24}$$

We will indicate the order of the ENO scheme in the form:

spaceorder — timeorder — ENO scheme .

3.2 Constant Coefficient Systems

We will now extend the spatial ENO approximation to liner systems with constant coefficients:

$$u_t + A u_x = 0 , \quad f = A\, u \tag{3.25}$$

We denote the matrix of the left and rigth eigenvectors by:

$$\begin{aligned} L^T &= (l_1 , l_2 , \ldots , l_d) \\ R &= (r_1 , r_2 , \ldots , r_d) \end{aligned} \tag{3.26}$$

and define the diagonal matrix of the eigenvalues by:

$$D = \mathbf{diag}\,(a_1 , a_2 , \ldots , a_d) \tag{3.27}$$

With appropriate scaling we obtain eigenvectors which are orthonormal:

$$L = R^{-1} \tag{3.28}$$

and the matrix A may be expressed as a transformed diagonal matrix:

$$A = R\, D\, L \tag{3.29}$$

A field by field decomposition of u decoupules the system (3.25):

$$w_t + D\, w_x = 0 , \quad w = L\, u \tag{3.30}$$

The decoupled flux is given by:

$$g = D\, w = L\, f \tag{3.31}$$

Now we apply the Lax-Friedrichs ENO scheme to each component seperately and define:

$$\begin{aligned} g^+ &= \tfrac{1}{2}\,(g + \beta |D|\, w) \\ g^- &= \tfrac{1}{2}\,(g - \beta |D|\, w) \end{aligned} \tag{3.32}$$

where:

$$1 \le \beta \le \frac{1}{a_i}\,\frac{\Delta x}{\Delta t} \tag{3.33}$$

Notice that the constant α of equation (3.14) is replaced by the quantity βa_i . The numerical fluxes are then obtained by the adaptive stencil operator (3.23) aplied on each component seperately:

$$\hat{g}^+_{j+½} = N^+_{j+½}\,(g^+_k)\,, \qquad k^{(r+1)}_{\min} \le k \le k^{(r+1)}_{\max} \tag{3.34}$$

We will restrict the formulation to the positive fluxes. The negative fluxes are approximated in an analogous manner.

Multiplication with the right eigenvectors transforms the decoupled flux into the original flux:

$$\hat{f}^+_{j+½} = R\ \hat{g}^+_{j+½} \tag{3.35}$$

Thus the flux may be formulated as:

$$\hat{f}^+_{j+½} = \frac{1}{2}\ R\ N^+_{j+½}\ (\,L\,f_k + \beta\,|D|\,L\,u_k\,) \qquad k^{(r+1)}_{\min} \le k \le k^{(r+1)}_{\max} \tag{3.36}$$

3.3 Nonlinear Systems

Formulation (3.36) is easily extended to nonlinear systems of hyperbolic conservation laws. We use a 'local linearisation' and define an average Jacobian at the cell interface $j+½$:

$$A_{j+½} = \frac{\partial f}{\partial u}(u_{j+½}) \tag{3.37}$$

Here we have several choices for the average Jacobian, i. e. we may take the Jacobian at the mean value:

$$A_{j+½} = A\,(\overline{u}_{j+½}) = A\,(½(u_j+u_{j+1})) \tag{3.38}$$

or we may take the Jacobian at the average $\tilde{u}_{j+½}$ introduced by Roe[25]:

$$A_{j+½} = A(\tilde{u}_{j+½}) \tag{3.39}$$

The numerical results in chapter 4 are obtained using the Roe average but numerical test gave the same results with the cheaper mean value Jacobian (3.38). The eigenvectors and eigenvalues of the average Jacobian will be denoted as:

$$L_{j+½}\ ,\ R_{j+½}\ ,\ D_{j+½} \tag{3.40}$$

Then we obtain the nonlinear version of the numerical flux (3.36):

RNDL-ENO scheme

$$\hat{f}^{+}_{j+½} = \frac{1}{2} R_{j+½} N^{+}_{j+½} \left(L_{j+½} f_k + \beta |D_{j+½}| L_{j+½} u_k \right) \qquad k^{(r+1)}_{\min} \le k \le k^{(r+1)}_{\max} \tag{3.41}$$

To avoid expansion shocks we may add some more numerical dissipation at sonic points thereby replacing $|D_{j+½}|$ by

$$|D_{j+½}| = \mathbf{diag}\left(\max(|a_{i\,j}|, |a_{i\,j+1}|) \right) \tag{3.42}$$

We now discuss the numerical work involved in calculating the fluxes. The adaptive stencil operators $N^{+}_{j+½}$ and $N^{-}_{j+½}$ chose the actual nodes in the range:

$$[j-r\ ,\ j+r+1] \tag{3.43}$$

where r is the order of the scheme. This gives a crude estimate of the number of matrix multiplications involved in calculating the flux of :

$$operations \approx 3 \times (2r) \tag{3.44}$$

This is a somewhat pessimistic estimate because the adaptive stencil operator does not check all possible nodes in that range. But even a more realistic estimate has to take into acount that this operator compares the divided differences of two candidates before it can add a new node to the stencil. Therefore this estimate might not be

reduced very much if the order is not too high. We also did not take into account the numerical work involved in calculating the flux f, the eigenvectors and the divided differences. For the one-dimensional gas dynamic equations, a multiplication with the three by three matrix $L_{j+½}$ costs about the same as the calculation of the flux f. The estimate (3.44) may be compared with the cost of the MacCormack scheme, which needs only one calculation of the flux. In the following chapter we present several more economical schemes, which need fewer matrix multiplications, but we will not change the adaptive stencil operator itself.

3.4 More Efficient Schemes

Here we will present simplifications which increase the efficiency of the RNDL-ENO scheme for nonlinear systems. Let us first assume that we may exchange the moving stencil operator $N_{j+½}$ and the matrix of the left eigenvectors $L_{j+½}$. Then we obtain the following

NRDL-ENO scheme:

$$\hat{f}^{+}_{j+½} = \frac{1}{2} N^{+}_{j+½} \left(f_k + R_{j+½} |D_{j+½}| L_{j+½} u_k \right) \qquad k^{(r+1)}_{\min} \le k \le k^{(r+1)}_{\max} \tag{3.45}$$

We do not claim that the exchange of operators is justified, but numerical tests showed that the results obtained with the NRDL-ENO scheme differ only slightly from the results obtained with the RNDL-ENO scheme. The number of marix multiplications is only reduced by one and therefore the NRDL-ENO scheme is not much more efficient than the RNDL scheme.

The NRDL-ENO scheme would be simplified drastically if we could interchange the matrices $R_{j+½}$ and $|D_{j+½}|$. In general this is not possible, but we may replace the diagonal matrix $|D_{j+½}|$ by a matrix with larger diagonals:

$$\alpha_{j+½} I \tag{3.46}$$

where:

$$\alpha_{j+½} = \max(|a_1|, |a_2|, \ldots, |a_d|)_{j+½}$$

and I is the identity matrix. We then obtain the following

NDRL-ENO scheme:

$$\hat{f}^+_{j+½} = \frac{1}{2} N^+_{j+½} (f_k + \alpha_{j+½} u_k)$$
$$k^{(r+1)}_{\min} \le k \le k^{(r+1)}_{\max} \tag{3.47}$$

which contains no matrix multiplications. Clearly, this procedure increases the amount of dissipation associated with slower wave speeds. This will be confirmed by the numerical results presented in chaper 4.2.

A further simplifiation could be obtained if we avoid the repeated multiplication of u_k by the local factor $\alpha_{j+½}$ for several nodes k. We try if it is possible to calculate this product only once at each grid point. This scheme will be denoted by

NFU-ENO scheme:

$$\hat{f}^+_{j+½} = \frac{1}{2} N^+_{j+½} (f_k + \alpha_k u_k)$$
$$\alpha_k = \max(|a_1|, |a_2|, \ldots, |a_d|)_k \tag{3.48}$$

The numerical results in chapter 4.3 show that the third order NFU-ENO scheme is not free of spurious numerical oscillations. A reduction of the spatial operator from three to two gave smooth results with only slightly reduced accuracy.

We now apply this idea to the NRDL-ENO scheme (3.45) and obtain the

NFA-ENO scheme:

$$\hat{f}^+_{j+½} = ½ N^+_{j+½} (f_k + R_k \, |D_k| \, L_k u_k) \tag{3.49}$$

The numerical results obtained by this scheme in chapter 4.3 show that we have less dissipation than with the NFU-ENO scheme, and we also had to reduce the spatial accuracy to obtain a smooth solution.

For the one-dimesional gas dynamic equations we are able to simplify the calculations for the NFA-ENO scheme. We will first assume that all eigenvectors of the Jacobian A are positive. Then we may simplify the second term in the brackets of formula (3.49):

$$R_k \, |D_k| \, L_k \, u_k = R_k D_k L_k \, u_k = A_k \, u_k = f_k \tag{3.50}$$

The last equation is a consequence of the Euler homogeneity relation (Courant Hilbert [26], p. 9) and the fact that the gas dynamic flux is homogeneous of degree one. Thus we obtain:

$$\hat{f}^{+}_{j+½} = N^{+}_{j+½} \, (f_k) \tag{3.51}$$

and:

$$\hat{f}^{-}_{j+½} = 0$$

In general the wave speeds a_i may obtain positive and negative values. We restrict the following calculations to the case that two wave speeds are positive and one, e. g. a_1 , is negative. Other possible combinations may be treated in a similar manner. We then simplify the scheme (3.49) using :

$$|a_1| = a_1 - 2a_1 \tag{3.52}$$

and:

$$|D| = D - 2\mathbf{diag}\,(a_1 , 0 , 0) \tag{3.53}$$

This gives:

$$(R \, |D| \, L)_k = (A - 2a_1 \, r_1 \, l_1^T)_k \tag{3.54}$$

and we obtain:

$$\begin{aligned} f_k^{-} &= (a_1 \, r_1 \, l_1^T \, u)_k \\ f_k^{+} &= f_k - f_k^{-} \end{aligned} \tag{3.55}$$

For the special case of the gas dynamic equations the calculation of f^- is very cheap. Many terms in the matrix products in equation (3.55) cancel and we obtain:

$$f^{-} = \alpha_1 \begin{bmatrix} \rho \\ \rho\,(v - c) \\ \rho\varepsilon + p - \rho v \, c \end{bmatrix} \tag{3.56}$$

where:

$$\alpha_1 = \min(a_1, 0.0) \tag{3.57}$$

This gives also a very simple scheme which includes no matrix multiplications.

4. Numerical Results

For two test problems a simple shock wave and the shock/turbulence interaction model of chapter 2 we compare the numerical results obtained with the MacCormack scheme [2], the TVD scheme of Davis [3] and the ENO versions of chapter 3. In all case the Mach number of the mean shock speed $M_{sh} = v_{sh}/c_1$ is 2.0, the step size Δx is 0.1 and the time step ratio $\Delta t/\Delta x$ is 0.25, which gives a CFL number of 0.65 in the simple shock case.

We add fourth order numerical dissipation similar to the nonlinear adaptive dissipation of Jameson and Schmidt [27] to the MacCormack scheme. (We omit the second dissipation term $\varepsilon^{(4)}$ of [27] p. 472). The dissipation is controlled by a constant ε (which is the constant $k^{(2)}$ in [27], p. 473).

4.1 Simple Shock Wave

Figure 2 to 5 show the density profiles for a simple Mach 2.0 shock wave. Initially the shock is at position 0.0; the final shock position is 4.0 .

Figure 2 shows the influence of the additional dissipation for the MacCormack scheme. The MacCormack scheme captures the shock and gives the correct shock position. Without additional dissipation ($\varepsilon = 0.0$) the scheme leads to considerable numerical oscillations behind the shock. With additional dissipation ($\varepsilon = 2.0$) these post shock oscillations are reduced but they are still present. In both cases the numerical shock profile is sharp and stretches over three grid spacings. Notice that the stars mark the shock profile. Numerical tests showed that it is not possible to reduce the

post shock oscillations totally without smearing the shock over too many grid points. The present result is therefore a compromise between a sharp shock profile and acceptable oscillations. The amount of necessary dissipation depends on the problem, the CFL number (i. e. the time step and the grid spacing) and personal preferences of the scientist.

In both cases we obtain numerical disturbances near $x = 0.0$ and $x \approx 2.0 - 3.0$. Further investigation showed that these disturbances are due to the discrepancies between the initial shock profile, which stretches over one grid spacing, and the numerical shock profile. There exists a characteristic, almost self similar, numerical shock profile which propagates through the grid. In the first few time steps the numerical scheme transforms the initial profile into a numerical profile, and emits an entropy disturbance travelling with approximately the flow speed v and a slow acoustic wave travelling with the speed $v-c$. In the present case this speed is –0.049 and therefore the acoustic disturbance moves to the left very slowly. We found similar numerical disturbances in the results of the other schemes (figure 3 to 5). For the shock turbulence interaction results in chapter 4.2 we used an initial shock profile generated by a preliminary calculation. This procedure avoided these numerical disturbances.

Figure 3 compares the result of Davis' TVD scheme [3] with the MacCormack scheme. The TVD scheme gives remarkable accurate results with no post shock oscillations. The TVD scheme has no free control parameters which have to be adapted to the problem. Both schemes show the equally sharp shock profiles.

The density profile obtained with the third order RNDL-ENO scheme of chapter 3.3 shows a sharp shock profile without post shock oscillations (figure 4). Let us now consider the results for two first order accurate RNDL-ENO schemes in figure 5. The first scheme, indicated by circles, uses only one node, the starting node, and approximates the positive and negative flux by a constant function. It is clear that this scheme is very dissipative and leads to a poor resolution of the shock. The second scheme,

indicated by a solid line and stars near the shock, uses two nodes and approximates the fluxes by a linear function. This is still only first order accurate in space. It is seen that this scheme leads to a remarkable sharp shock profile. Further investigation shows that this is a consequence of a compressive mechanism of this first order scheme.

Results for a scalar, constant coefficient hyperbolic equation

$$u_t + u_x = 0 \tag{4.1}$$

with sine wave and zigzag wave initial conditions and periodic boundary conditions are presented in figure 6 and 7. We present the initial profiles and the solutions after four periods. The inherent dissipation of the constant polynomial scheme (figure 6), which in the present case is identical to a first oder upwind scheme, reduces the amplitude of the sine wave and smears the zigzag wave considerably. On the other hand, the linear polynomial scheme (figure 7) steepens the gradients and transforms the initial waves to a step wave. This property is lost if we increase the order of the time marching procedure. The averaging procedures of the second and third order Runge-Kutta time marching schemes removes the steepening trends.

4.2 Shock / Turbulence Interaction

We now discuss the numerical results for the shock/turbulence interaction model. Figure 8 shows the pressure and density profiles of the a numerical solution obtained with the third order RNDL-ENO sheme of chapter 3.3 using a fine grid with 951 points. This high resolution solution will be referred to as the exact solution. We show the initial (numerical) shock profiles and the profiles after the time which a shock, running with the mean speed v_{sh}, needs to pass four wavelength of the density wave. The pressure profile shows four wavelengths of the left running acoustic wave generated by the interaction process. It is clearly seen that this wave steepens to left running

shocks. This steepening process, together with the interaction of the shock with the density wave generates a kink near $x = 12$. The small disturbance near $x = 14$ seems to be a numerical disturbance. In the density profile only the two leftmost acoustic waves are clearly visible. Just behind the shock we see four waves of the entropy wave generated by the shock. The amplitude of this wave is considerably larger than the amplitude of the impinging wave ahead of the shock. There is also a modulation of the entropy wave behind the shock which is due to the acoustic wave. Near $x = 10$ we have an interaction between a shock produced by the steepening of the acoustic wave and the tail of the entropy wave. Notice that the entropy wave is not visible in the pressure profile. The shock profiles indicated by the stars consist of only one or two points and are extremely sharp.

For various schemes we will now compare the numerical results obtained with a grid consisting of 191 points and the fine grid 'exact' solution. Figure 9 shows the results for the MacCormack scheme with additional numerical dissipation ($\varepsilon = 2.0$). The pressure profile is in good agreement with the exact solution, but the details near $x = 12$ are not resolved with this coarser mesh. We also see post shock oscillations behind the strong right running shock. The numerical shock profile contains two to three points. The density profile shows that the amplitude of the entropy wave is smaller than for of the fine grid solution. This could have been expected. But it is surprising that the wavelength is not represented correctly by the MacCormack scheme. Control calculations with a 951 grid gave the correct wavelength, but numerical oscillations were still present. For the grid of 191 points the intraction between the tail of the entropy wave and the steepening acoustic wave is not represented. We obtain large numerical oscillations in that region. As the numerical dissipation added to the MacCormak scheme is controlled by the gradients of the pressure, these density oscillations are not damped. But it would be difficult to control these oscillations without effecting the entropy wave, because these numerical oscillations have large

wavelength and gradients of the same order than the entropy wave.

The numerical solution obtained with Davis' TVD version [3] of the MacCormack scheme is presented in figure 10. There are small numerical oscillations behind the left running shocks. This cold be due to the simple TVD algorithm which avoids the field by field decomposition of the flow into the eigenvectors. The strong right running shock has no oscillations. The scheme does not resolve the details near $x = 12$. The density profile shows that the wavelength of the entropy wave is accurately resolved but the amplitude is considerably reduced. This is due to the loss of accuracy of TVD schemes near extrema. The oscillations near the tail of the entropy wave are much smaller than in figure 9, but the interaction of the entropy wave with the steepening acoustic wave is not resolved accourately. The numerical shock profiles contain two to three points.

The comparison of the results for the third order RNDL-ENO scheme obtained for a grid of 191 points with the fine grid solution in figure 11 shows the remarkable good accuracy obtained by the coarse grid. There is only a slight loss of accuracy. The shock profiles are sharp and contain only one to two points.

Figure 12 shows that exchanging the spatial ENO adaptive stencil operator N and the matrix of eigenvectors R does not change the solution. The results obtained with the third order RNDL-ENO scheme are almost identical with the results obtained with the third order NRDL-ENO scheme defined in chapter 3.3. Both schemes need about the same amount of computation time.

In figure 13 results obtained by the NDRL-ENO scheme are compared with results of the RNDL-scheme. The pressure profiles show that there are no differences at the right running fast shock. Even the shock profile is almost identical. For the left running shocks we observe a slightly larger smearing of the shock profiles by the

NDRL-ENO scheme. There are about four points in the shock. This could be expected because in constructing the NDRL-ENO scheme we increased the wave speeds of the slow waves thereby increasing the numerical dissipation associated with these waves. We also observe more dissipation in the entropy wave following the shock. The amplitudes of the entropy wave for the NDRL-ENO scheme are smaller than for the RNDL-ENO scheme. Notice that there is no increase of dissipation for the right running shock.

Figure 14 clarifys the relations between the wave speeds. The absolute values of the eigenvalues of the Jacobian (3.2), normalized with the sound speed c are shown as a function of the flow speed v. For the present problem of a Mach 2.0 shock we obtain a flow speed of $0.96\,c$ behind the shock. The Mach number of the flow behind the shock is therefore close to 1.0 and the slowest wave speed is almost zero. On the other hand, the fasted wave speed is almost 2.0. We therefore increase the dissipation by replacing the slow wave speeds with the fastest wave speed. Figure 14 shows that the present problem is almost the worst case. For most other flow Mach numbers, the difference between the maximal amd minimal wave speed is smaller. The result in figure 13 is therefor a very dissipative case. For other shock speeds, expecially for fast shocks, we might expect less dissipative shock profiles.

4.3 Results for the NFA-ENO and NFU-ENO Schemes

In figure 15, We compare the results for the even more economical NFU-ENO schemes with the NDRL-ENO schemes. Both are in close agreement with each other and the shock profiles are spraed over the same distance. But there are some numerical disturbances in the NFU-ENO data. These could be removed by reducing the order of the spatial adaptive stencil operators $N^{+}_{j+½}$ and $N^{-}_{j+½}$. We kept the third order Runge-Kutta time discretisation because a reduction to second order gives to much dissipation near the shocks. The result for the second order NFU-ENO scheme is

presented in figure 16. The pressure and density profiles are smooth and in good agreement with the third order NDRL-ENO scheme. The amplitude of the entropy wave and small details of the profiles are not accurately represented by the second order scheme due to the reduced accuracy.

We now compare the EFA-ENO scheme with the NRDL-ENO scheme. Here again, numerical disturbances are obtained with the third order EFA-ENO scheme. We only present the results for the second order scheme in figure 17 and 18. The pressure and density profiles are in close agreement with the much more expensive third order NRDL-ENO scheme. The shocks are pretty sharp but the maxima of the left running shock profiles are sligthly more smoothed than with the NRDL-ENO scheme. The NFA-ENO scheme seems to be more dissipative in subsonic flow regions than in supersonic regions. For the present problem, the flow is subsonic near the maxima of the shock profiles and supersonic near the minima. We also observe small expansion shocks near sonic points of the solution. At the present stage of the work we are not able to avoid these expansion shocks.

Finally we will apply the NFA-ENO scheme to a shock turbulence interaction problem with a mean shock Mach number of 3.2 (figure 18). For this problem the mean flow behind the shock is supersonic and we expect sharp shock profiles and no expansion shocks. The results of the NFA-ENO scheme show no expansion shocks and are in excellent agreement with the third order RNDL-ENO sheme. Notice that we supress the data for the RNDL-ENO scheme in regions where both shemes give identical results. Only the amplitude of the entropy wave is sligthly smaller than for the field by field decomposition RNDL-ENO scheme, and we found a very small numerical disturbance in the pressure profile of the NFDA-ENO scheme which is not present in the RNDL-ENO data. The shock profiles of both schemes are sharp.

In the present stage of the investigation we have not optimized the programms for the various scheme. Therefor we do not present a comparison of the computational time required by the different schemes. This would have been unfair for the more complicated schemes which are much harder to optimise.

5. Summary

Efficient implementations of Runge-Kutta ENO schemes based on the Lax-Friedrichs building block (Shu and Osher [1]) for hyperbolic systems of conservation laws are discussed. There are two causes which make ENO schemes expensive. One is the nonlinear adaptive stencil principle, which is essential for the excellent shock capturing properties of the schemes. The second, relevant only for nonlinear systems, is the field by field decomposition of the flux. We present several more economic ENO schemes, which reduce or avoid the numerical work involved with this decomposition. This makes ENO schemes much faster and more competitive.

The new schemes are applied to two gas dynamical test problems, a simple shock wave, and the interaction of a shock with an entropy wave, which is regarded as a simplified model of shock/turbulence interaction. The solution of the second test problem possesses a complicated structure, but is still simple enough to be useful as a one-dimensional test problem. Results obtained with the new economical ENO schemes are compared with the field by field decomposition ENO scheme, the MacCormack scheme [2] with additional nonlinear viscosity [27], and Davis' TVD version of the MacCormack scheme [3].

All the schemes are adequate to calculate the simple shock problem, and the steepness of the numerical shock profiles are approximately the same. The additional

numerical viscosity of the MacCormack scheme damped the post shock oscillations sufficiently when the control parameter was adjusted to the problem. The TVD scheme and the ENO schemes are free of numerical oscillations.

The results for the shock/turbulence interaction show that the MacCormack scheme gives an incorrect answer unless a very fine grid is used. Small post shock oscillations, and large numerical oscillation behind the tail of the entropy wave, are observed. Furthermore the wavelength of the entropy wave and the interaction between the shocks and the tail of the entropy wave is not represented correctly. The solution obtained with the TVD scheme of Davis [3] gives the correct wavelength for the entropy wave, but the amplitude is clipped. The interaction between shocks and the tail of the entropy wave is distorted, and small numerical oscillations are present. The results of the ENO schemes show only very small numerical oscillations. The wavelength and amplitude of the entropy wave and the interactions between the tail of the wave and shocks is resolved correctly.

Results for the simple and fast NDRL-ENO scheme (which avoids a field by field decomposition of the flux) are as accurate as results for the much more expensive field decomposition RNDL-ENO scheme, and show only slightly increased smearing of the slow running shocks. It should be remarked that the shock/turbulence interaction with a Mach 2.0 shock is a crucial test, because the differences between the slowest and fastest wave speeds are almost maximal.

The even more economical NFU-ENO and NFA-ENO schemes require a reduction of the spatial order to produce smooth solutions. Results of the NFU-ENO scheme are only slightly more dissipative than the NDRL-ENO scheme. The NFA-ENO scheme gives steep shock profiles. For that scheme we obtained an accurate solution for a Mach 3.2 shock/turbulence interaction, but for a Mach 2.0 problem we observed small expansion shocks. We were not able to remove these expansion shocks at the present stage of the investigation.

The calculation of complex flows requires numerical schemes which are able accurately to calculate complex flow structures. The field by field decomposition version of the ENO scheme gives the most reliable and accurate result, but this scheme is also the most expensive in the present investigation. More economical ENO schemes with only slightly reduced accuracy are presented. Further simplifications and optimisations, as for example was begun by Shu and Osher [14], are mandatory.

Acknowledment

Many fruitful discussions with our colleagues Mao De-kang and Daniel Goovaerts are gratefully acknowledged.

6. References

[1] Shu Chi-Wang, Osher, S.: *Efficient Implementation of Essentially Non-Oscillatory Shock Capturing Schemes.* ICASE Report No. 87-33, 1987, to appear.

[2] MacCormack, R. W., Baldwin, B. S.: *A Numerical Method for Solving the Navier-Stokes Equations with Application to Shock-Boundary Layer Interactions.* AIAA paper 75-1, 1975.

[3] Davis, S. F.: *TVD Finite Difference Schemes and Artificial Viscosity.* ICASE Report 84-20, 1984.

[4] Owczarek, J. A.: *Fundamentals of Gas Dynamics.* Scranton, PA: Int. Textbook Comp., 1964

[5] Lax, P. D.: *Hyperbolic Systems of Conservation Laws and the Mathematical Theory of Shock Waves.* SIAM Conf. Series Lectures in Applied Mathematics

Vol. 11. Philadelphia, PA: SIAM, 1972.

[6] Sod, G. A.: *A Survey of Several Finite Difference Methods for Systems of Non-linear Hyperbolic Consevation Laws.* J. Comp. Physics, 27, 1978, pp. 1-31.

[7] Harten, A.: *On a Class of High Resolution Total-Variation-Stable Finite-Difference Schemes.* SIAM J. Numer. Anal. 21, 1983, pp. 1-23.

[8] Sweby, P. K.: *High Resolution Schemes Using Flux Limiters for Hyperbolic Conservation Laws.* SIAM J. Numer. Anal. 21, 1984, pp. 995-1011.

[9] Jameson, A., Lax, P. D.: *Conditions for the Construction of Multi-Point Total Variation Diminishing Difference Schemes.* Applied Numer. Math. 2, 1986, pp. 335-345.

[10] Osher, S., Chakravarthy, S.: *Very High Order Accurate TVD Schemes.* In: "Oszillation Theory, Computation and Methods of Compensated Compactness". IMA Vol. 2. Eds. Dafermos et al. 19**, pp. 229-274.

[11] Harten, A., Osher, S.: *Uniformly High-Order Accurate Non-Oscillatory Schemes I.* Univ. of Wisconsin, MRC Rep. No. 2823, 1985. (to apper in SIAM J. Numer. Anal.)

[12] Harten, A., Osher, S., Engquist, B., Chakravarthy, S. R.: *Some Results on Uniformly High Order Accurate Essentially Non-Oscillatory Schemes.* Applied Numer. Math. 2, 1986, pp. 347-377.

[13] Harten, A., Engquist, B., Osher, S., Chakravarthy, S. R.: *Uniformly High Order Accurate Essentially Non-Oscillatory Schemes, III.* J. Comp. Physics, 71, 1987, pp. 231-303.

[14] Shu Chi-Wang, Osher, S.: *Efficient Implementation of Essentially Non-Oscillatory Shock Capturing Schemes, II.* to appear .

[15] Osher, S., Sweby, P. K.: *Recent Developments in the Numerical Solution of Non-Linear Consercation Laws.* to appear.

[16] Katzer, E., Reister, H., Oertel jr., H.: *Numerical Simulation of Steady and Unsteady Shock Boundary Layer Interaction.* Fifteenth Int. Sympos. on Shock Waves and Shock Tubes, Berkley, CA, 1985; Proc. Stanford, CA: Stanford Univ. Press, 1986, pp. 487-493.

[17] Reister, H.: *Numerische Simulation der Wechselwirkung von Druckwellen mit laminaren und turbulenten Grenzschichten. (Numerical Simulation of the Interaction Between Pressure Waves and Laminar and Turbulent Boundary Layers.)* Deutsche Forschungs- und Versuchsanstalt für Luft- und Raumfahrt, Köln, West Germany; Report: DFVLR-FB 87-18, 1987.

[18] Katzer, E.: *Numerische Untersuchung der laminaren Stoß-Grenzschicht-Wechselwirkung.* Deutsche Forschungs- und Versuchsanstalt für Luft- und Raumfahrt, Köln, West Germany; Report: DFVLR-FB 85-34, 1985. (English translation: *Numerical Study of Laminar Shock/Boundary Layer Interaction.* European Space Agency, ESA-TT-958, 1986)

[19] Delery, J., Marvin, J. D.: *Shock-wave boundary layer interactions.* AGARD-ograph, AGARD-AG-280, 1986.

[20] Zang, T. A., Hussaini, M. Y., Bushnell, D. M.: *Numerical Computations of Turbulence Amplification in Shock-Wave Interactions.* AIAA Jounal, 22, 1984, pp. 13 - 21.

[21] Haas, J.-F., Sturtevant, B.: *Interaction of Weak Shock Waves with Cylindrical and Spherical Gas Inhomogeneities*. J. Fluid. Mech. 181, 1987, pp. 41-76.

[22] Hesselink, L., Sturtevant, B.: *Propagation of Weak Shocks Through a Random Medium*. to appear.

[23] McKenzie, J. F., Westphal, K. O.: *Interaction of Linear Waves with Oblique Shock Waves*. Physics of Fluids 11, 1968, pp. 2350-2362.

[24] Hildebrand, F. B.: *Introduction to Numerical Analysis*. New York, N.Y.: McGraw-Hill, 1956.

[25] Roe, P. L.: *The Use of the Rieman Problem in Finite Difference Schemes*. Seventh Int. Conf. on Num. Meth. in Fluid Dynamics, Stanford 1980. Proc., Berlin, Heidelberg, N. Y.: Springer, 1981.

[26] Courant, R., Hilbert, D.: *Methoden der mathematischen Physik, Band 2*. Berlin: Springer, 1937. (*Methods of Mathematical Physics, Vol. 2*. N. Y., London: Interscience Publ., 1962.)

[27] Jameson, A., Schmidt, W.: *Some Recent Developments in Numerical Methods for Transonic Flows*. Computer Methods in Applied Mechanics and Engineering, 51, 1985, pp. 467-493.

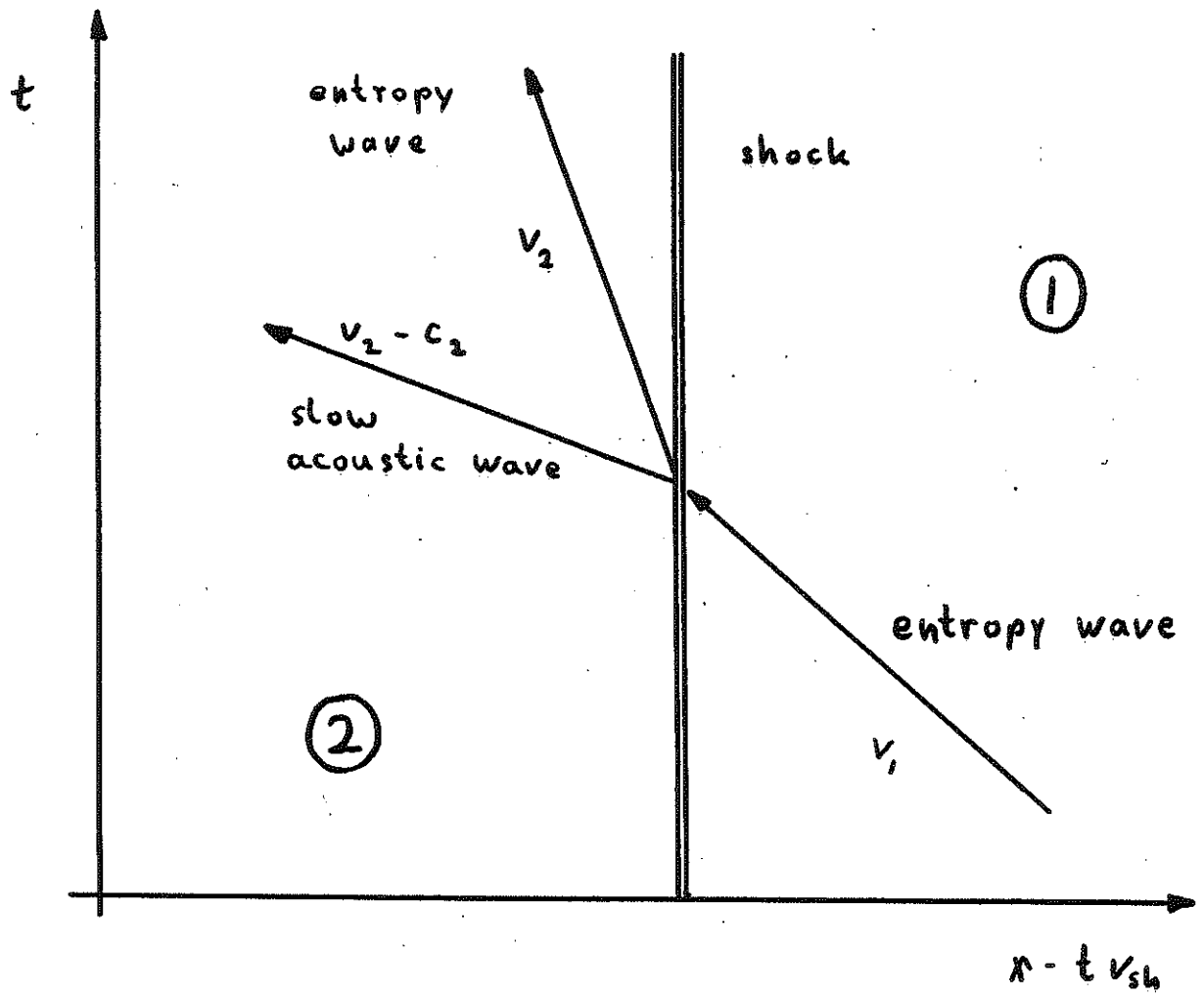

Fig. 1 : Linear shock / turbulence interaction

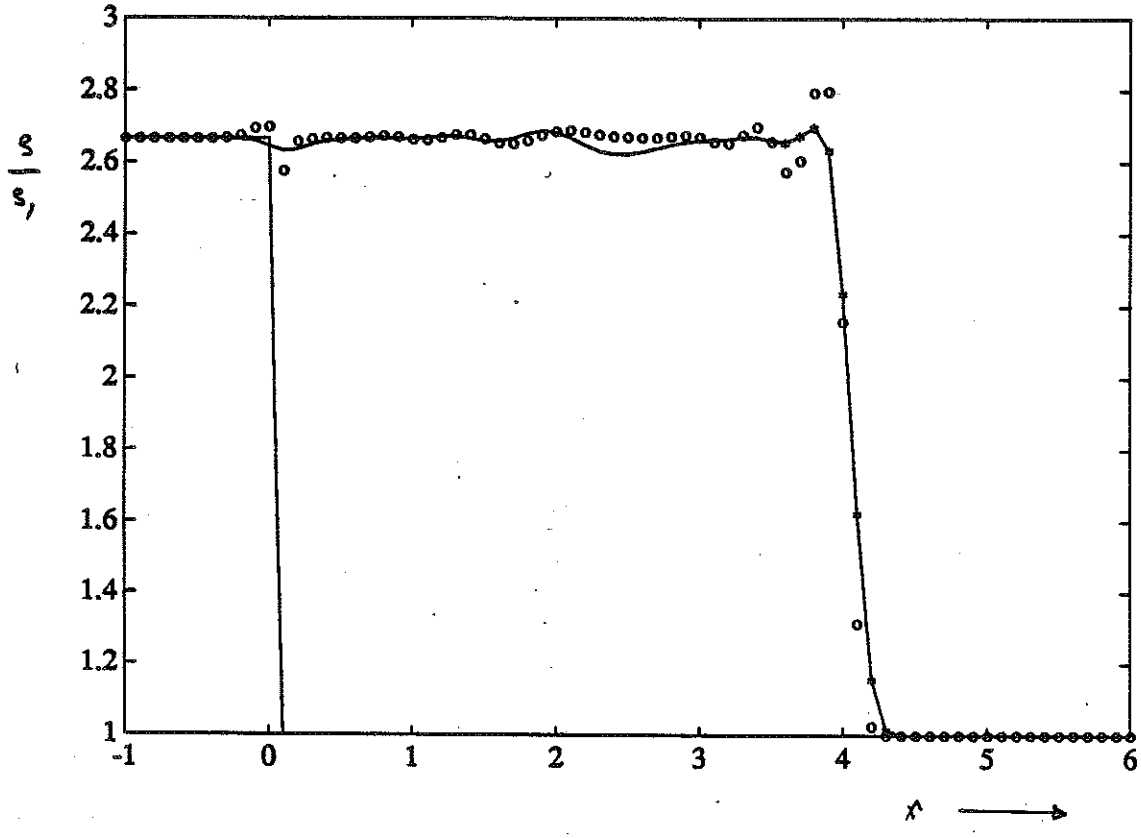

Fig. 2: Simple shock wave, $M_{sh} = 2.0$, $x_{sh} = 4.0$

—x— MacCormack scheme, $\varepsilon = 2.0$,

o o o o " " , $\varepsilon = 0.0$.

$\Delta x = 0.1$, $\Delta t/\Delta x = 0.25$, CFL # = 0.65

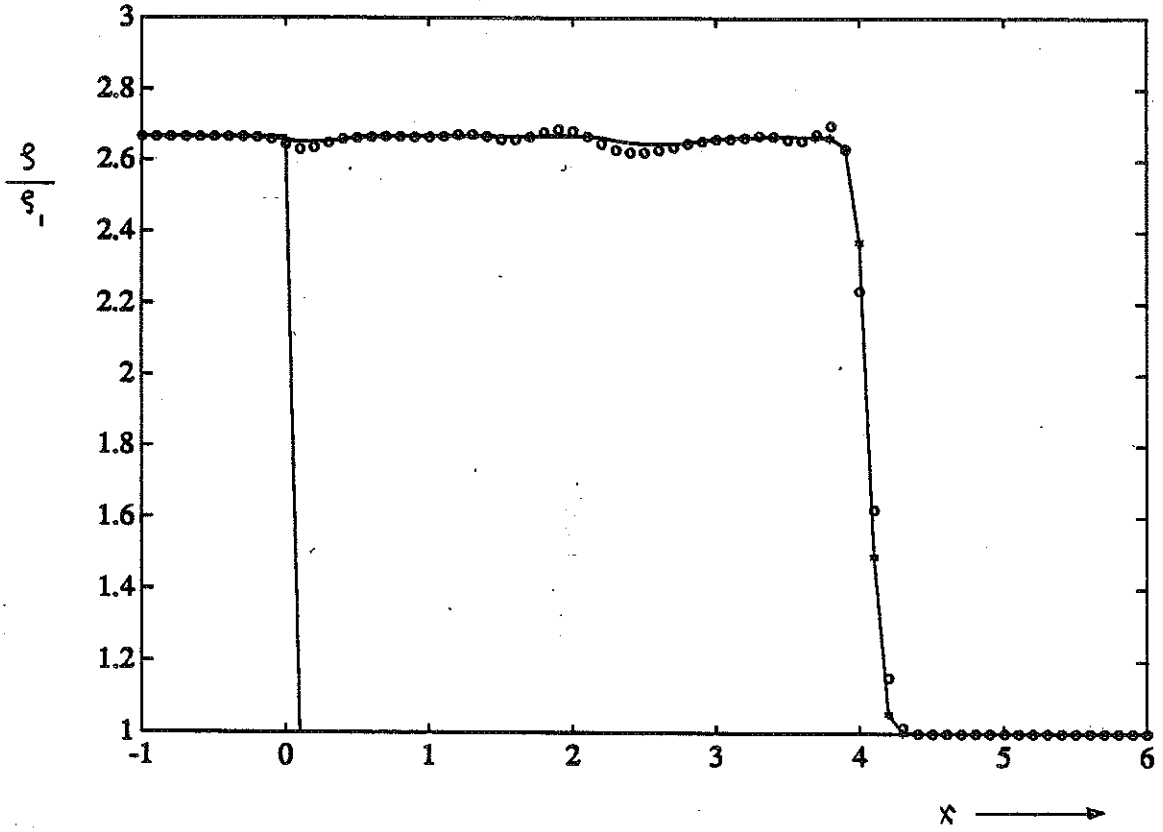

Fig. 3: Simple shock wave, $M_{sh} = 2.0$, $x_{sh} = 4.0$

—*— : Davis TVD scheme, oooo = MacCormack scheme,

$\varepsilon = 2.0$, $\Delta x = 0.1$, $\Delta t/\Delta x = 0.25$, CFL # = 0.65

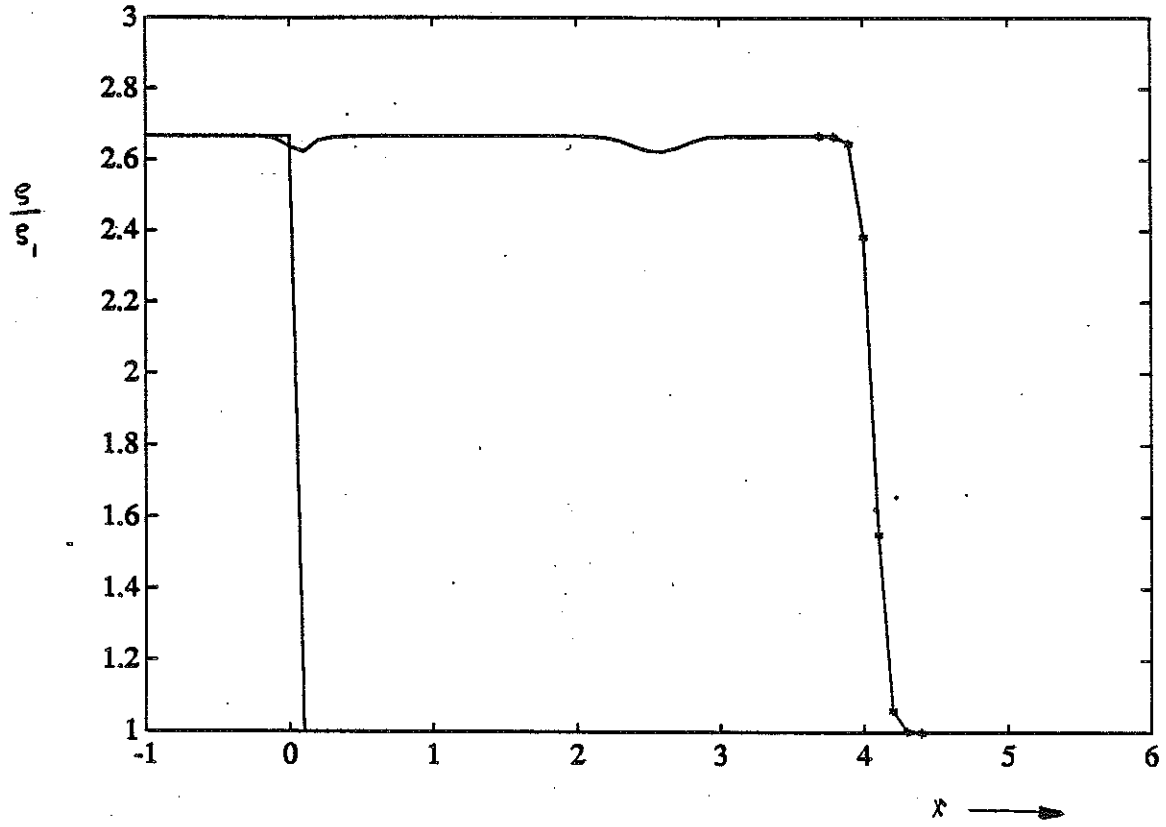

Fig. 4 : Simple shock wave, $M_{sh} = 2.0$, $x_{sh} = 4.0$

—×— : 3-3 RNDL-ENO scheme

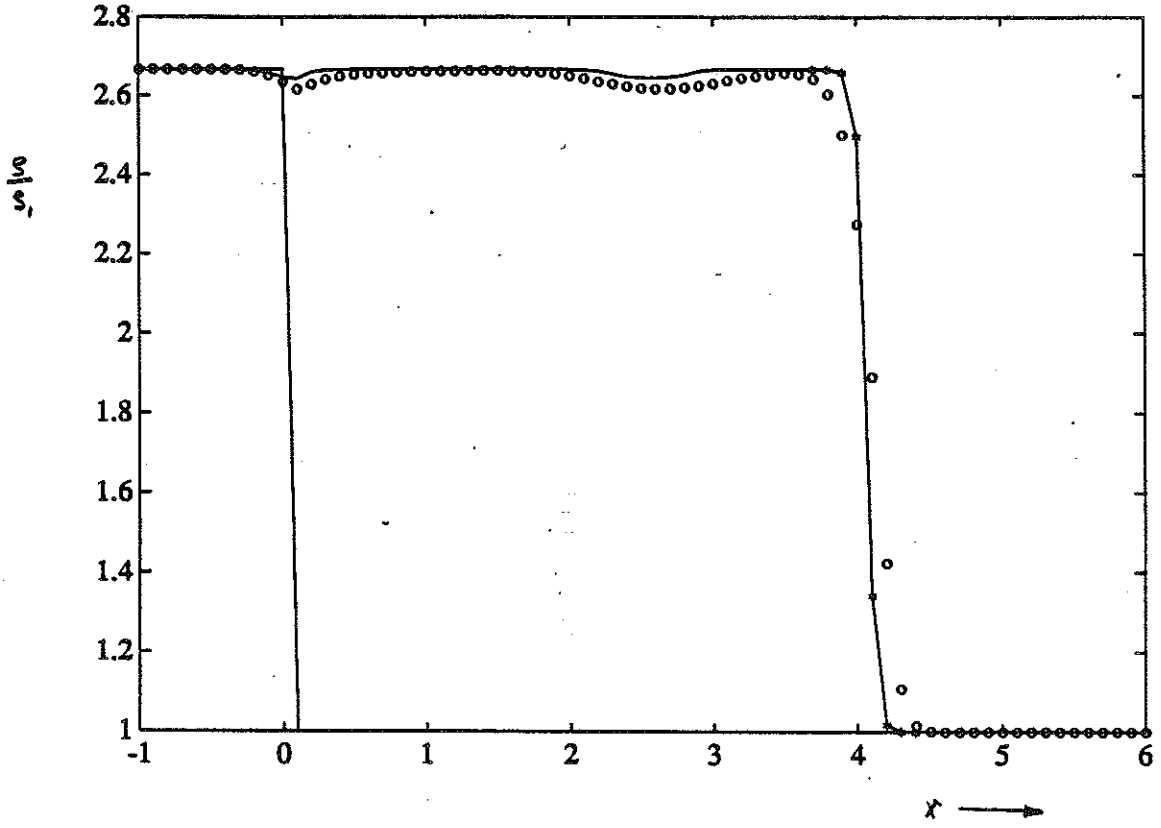

Fig. 5: Simple shock wave, $M_{sh} = 2.0$, $x_{sh} = 4.0$

1-1 RNDL-ENO scheme.

oooo : constant polynomial in space

—x— : linear polynomial in space

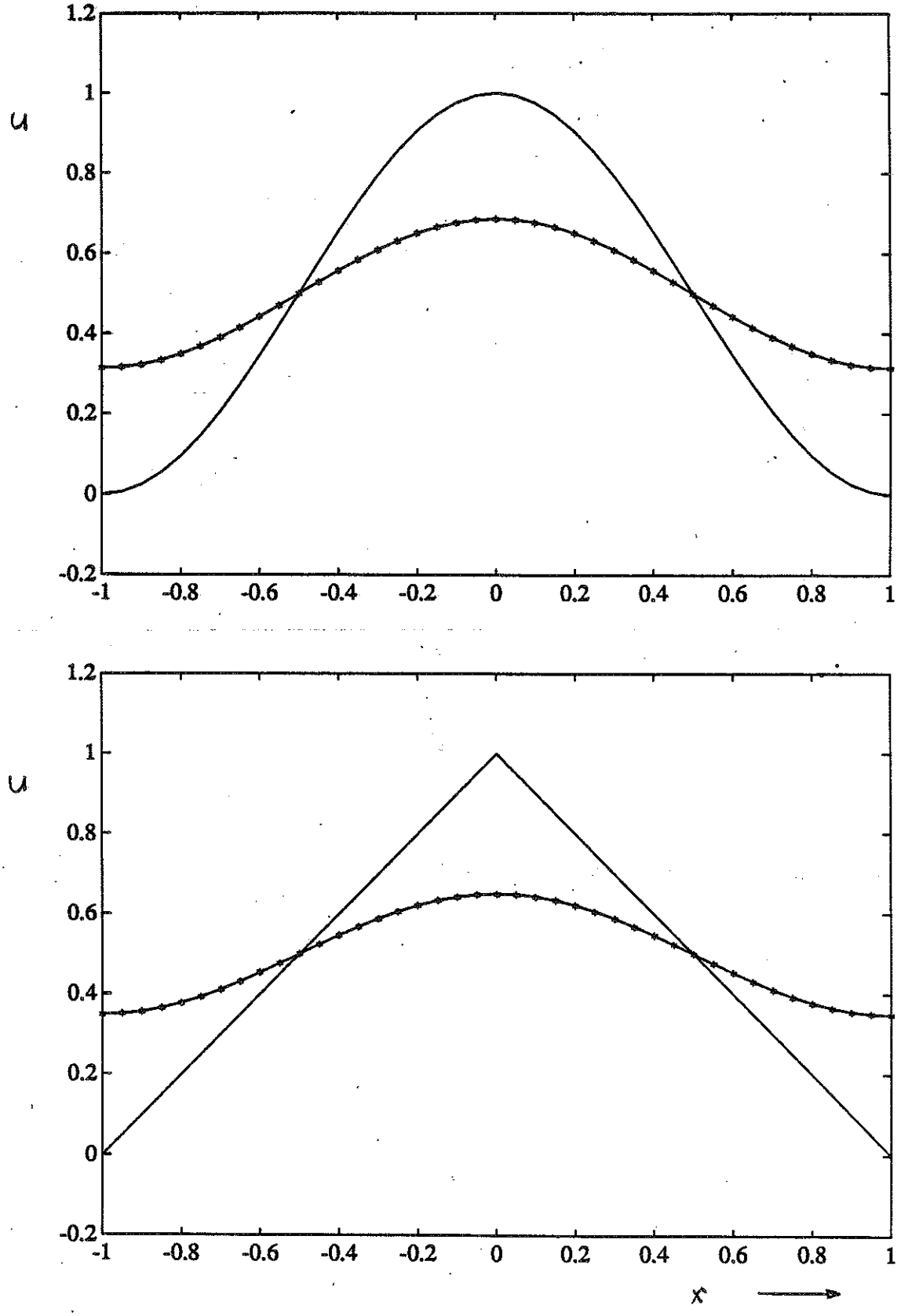

Fig. 6 : Diffusion of a sine and a zigzag wave after four periods; -*-. First order upwind scheme. —— : initial cond

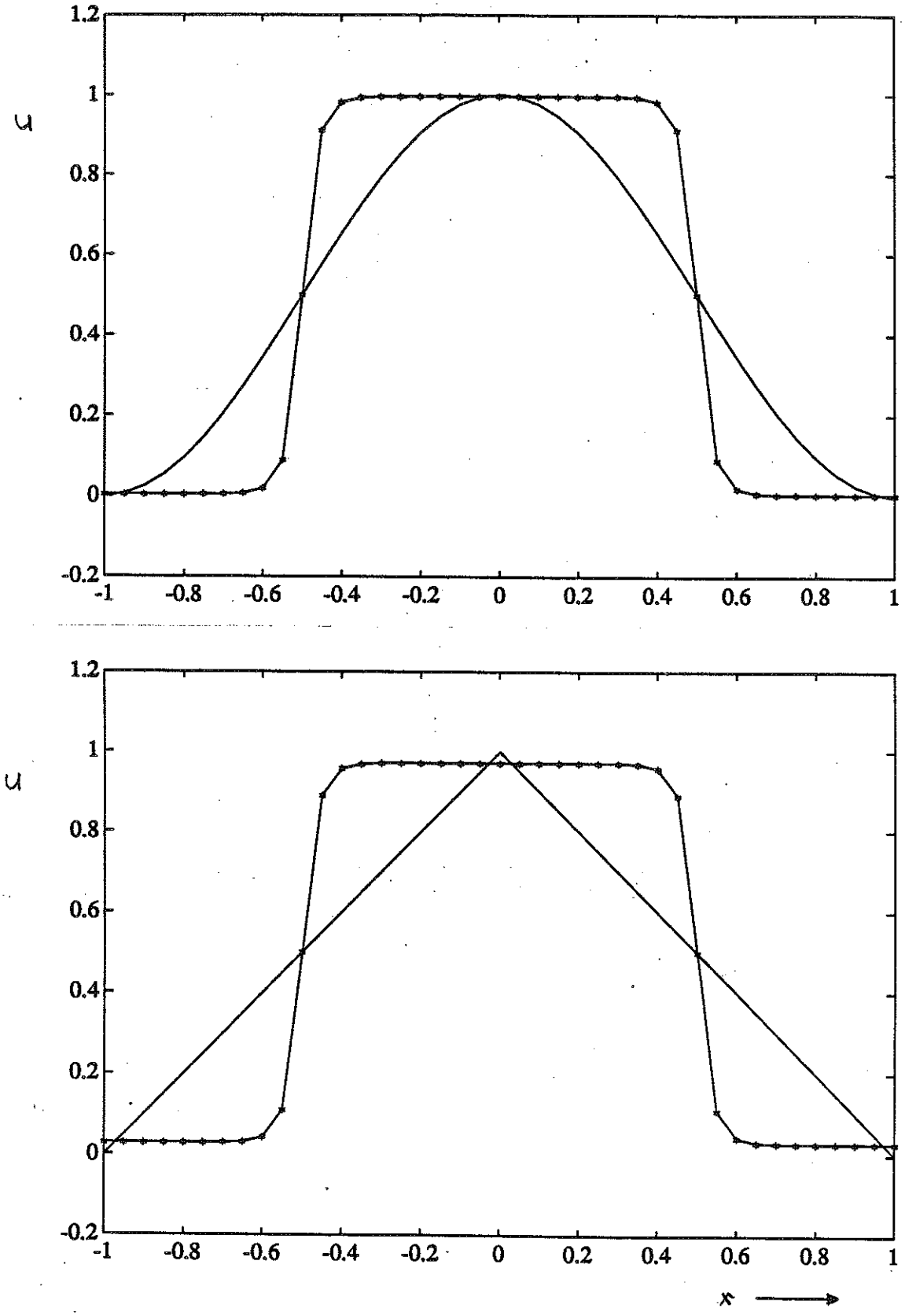

Fig. 7: Steepening of a sine and a zigzag wave after four periods. First order, linear polynomial ENO-scheme. ——— : initial value, —×— : final solution.

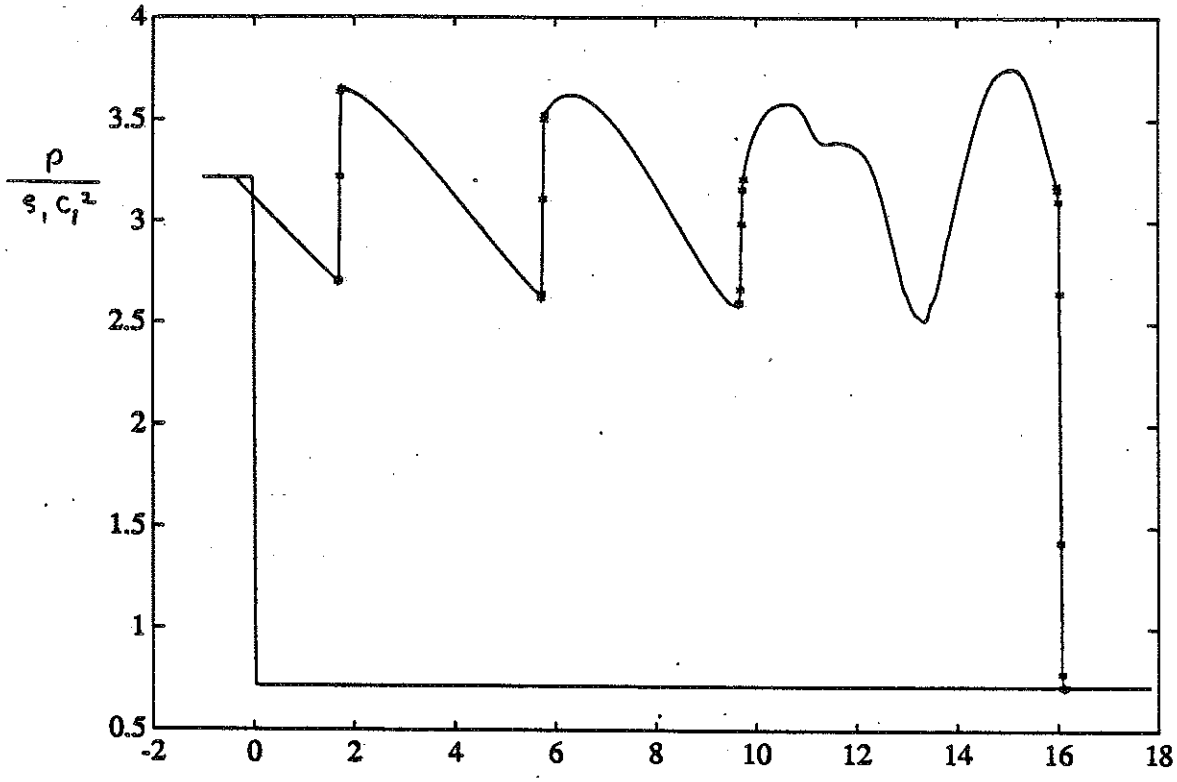

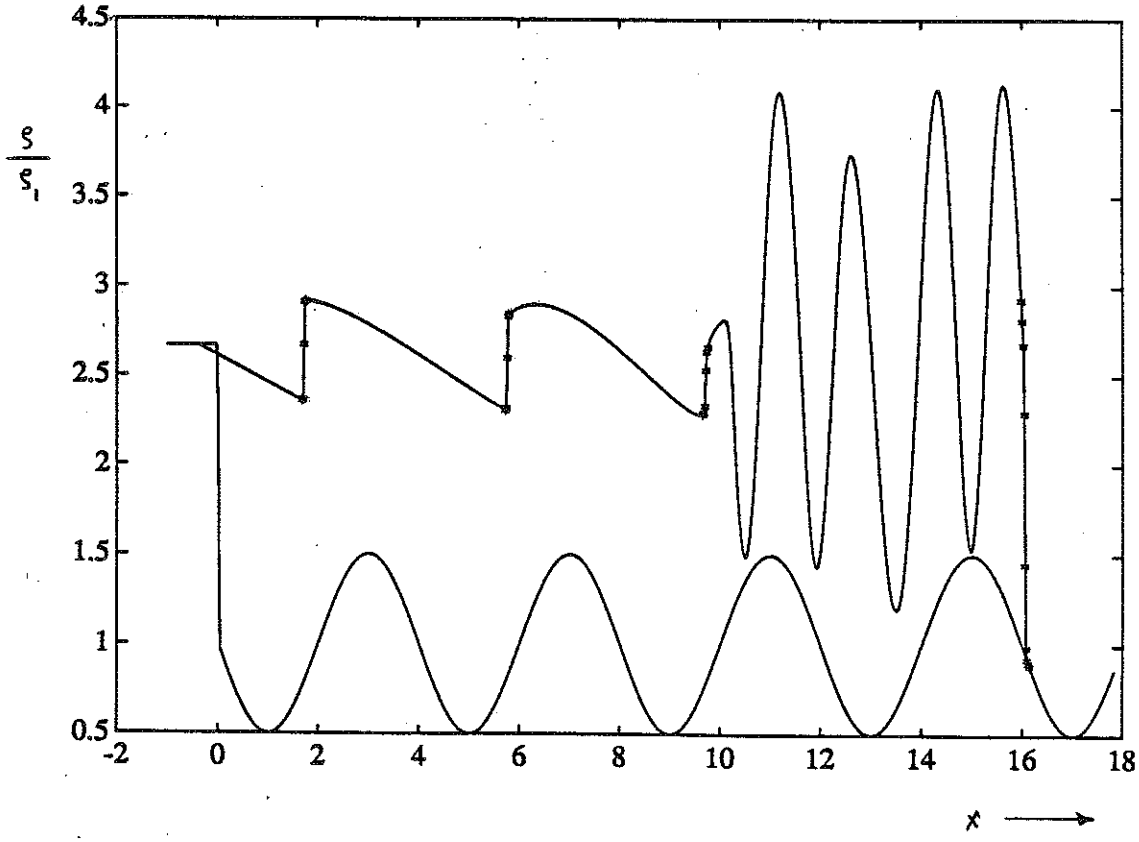

Fig. 8 : Shock / turbulence interaction, $M_{sh} = 2.0$, 3-3 RNDL-ENO scheme, $\Delta x = 0.02$, $\Delta t/\Delta x = 0.25$

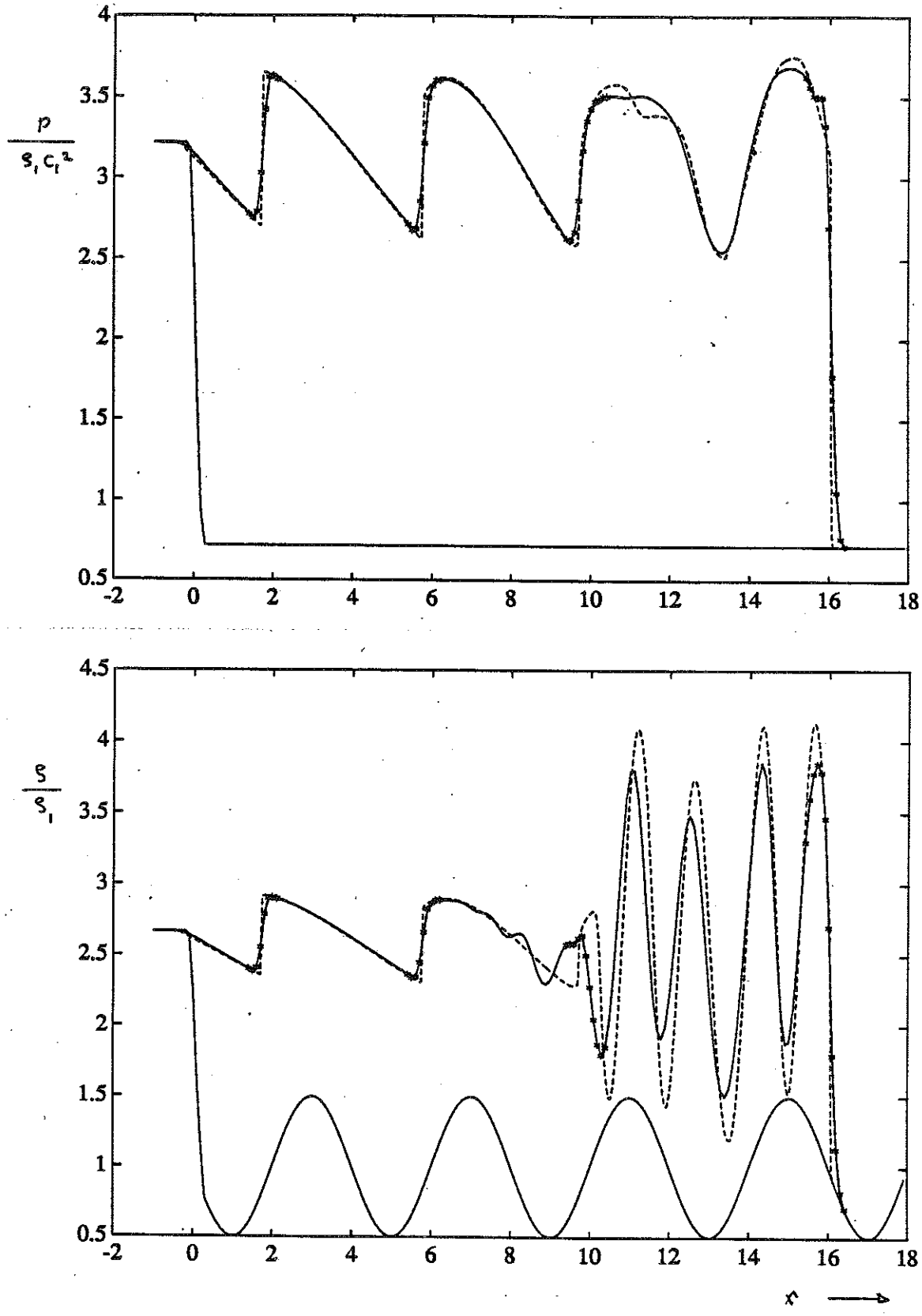

Fig. 9 : Shock/turbulence interaction, $M_{sh} = 2.0$
—x— : MacCormack, $\Delta x = 0.1$, $\Delta t/\Delta x = 0.25$, ---- : exact sol.

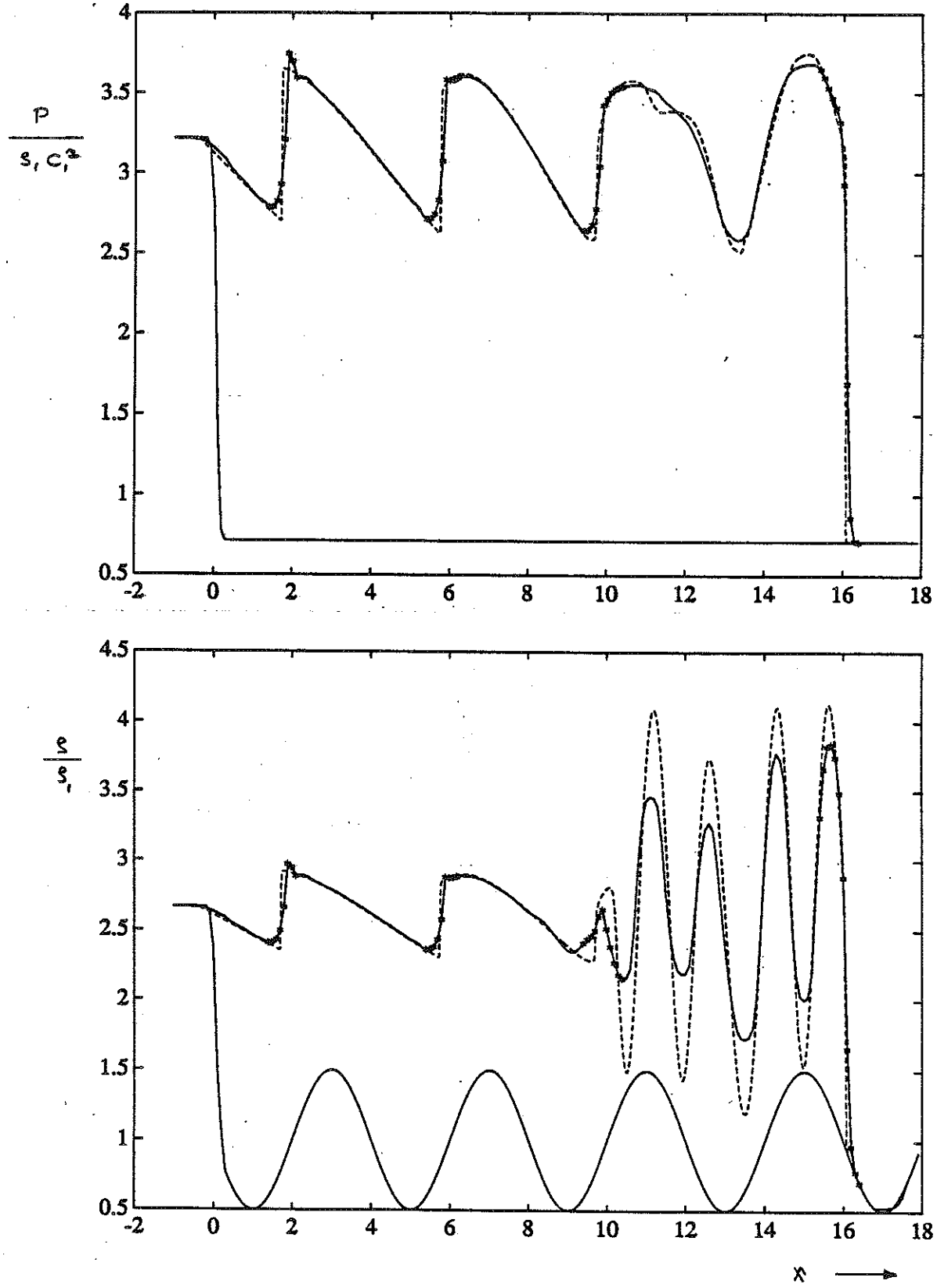

Fig. 10 : Shock / turbulence interaction. $M_{sh} = 2.0$,
——— : Davis TVD scheme, $\Delta x = 0.1$, $\Delta t / \Delta x = 0.25$, ---- : exact sol.

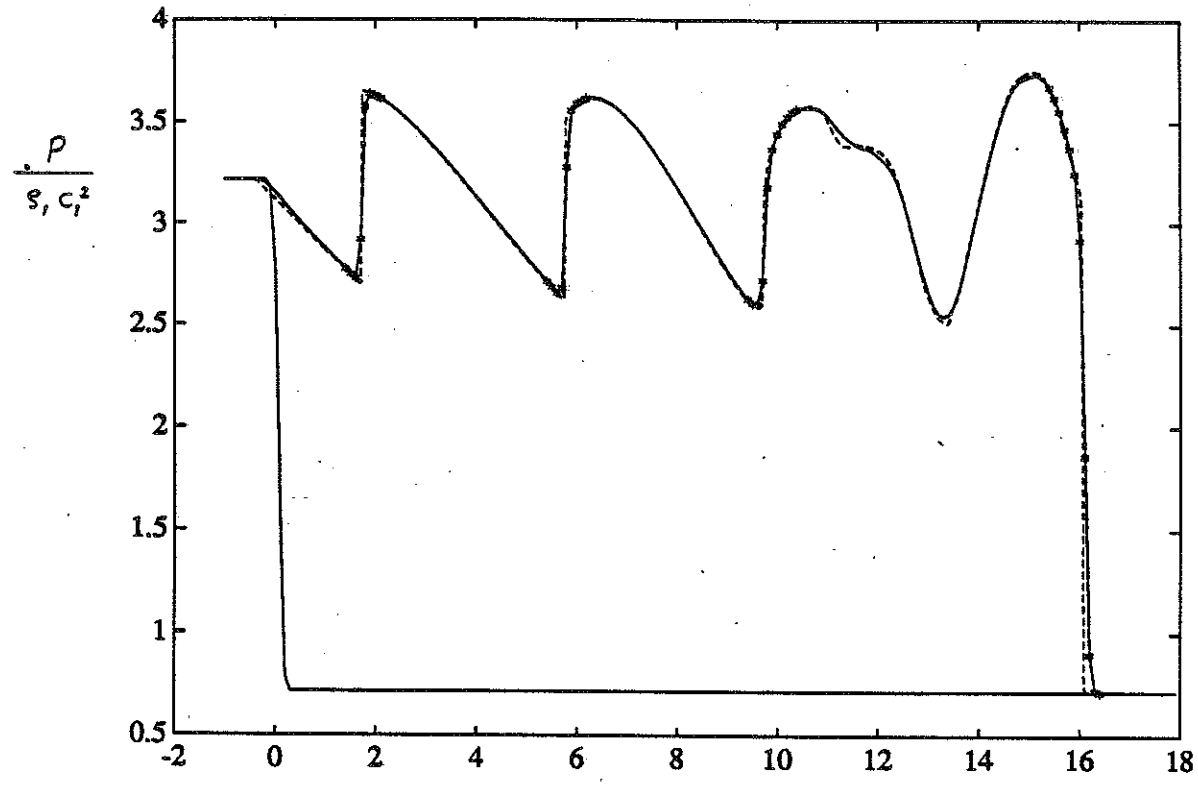

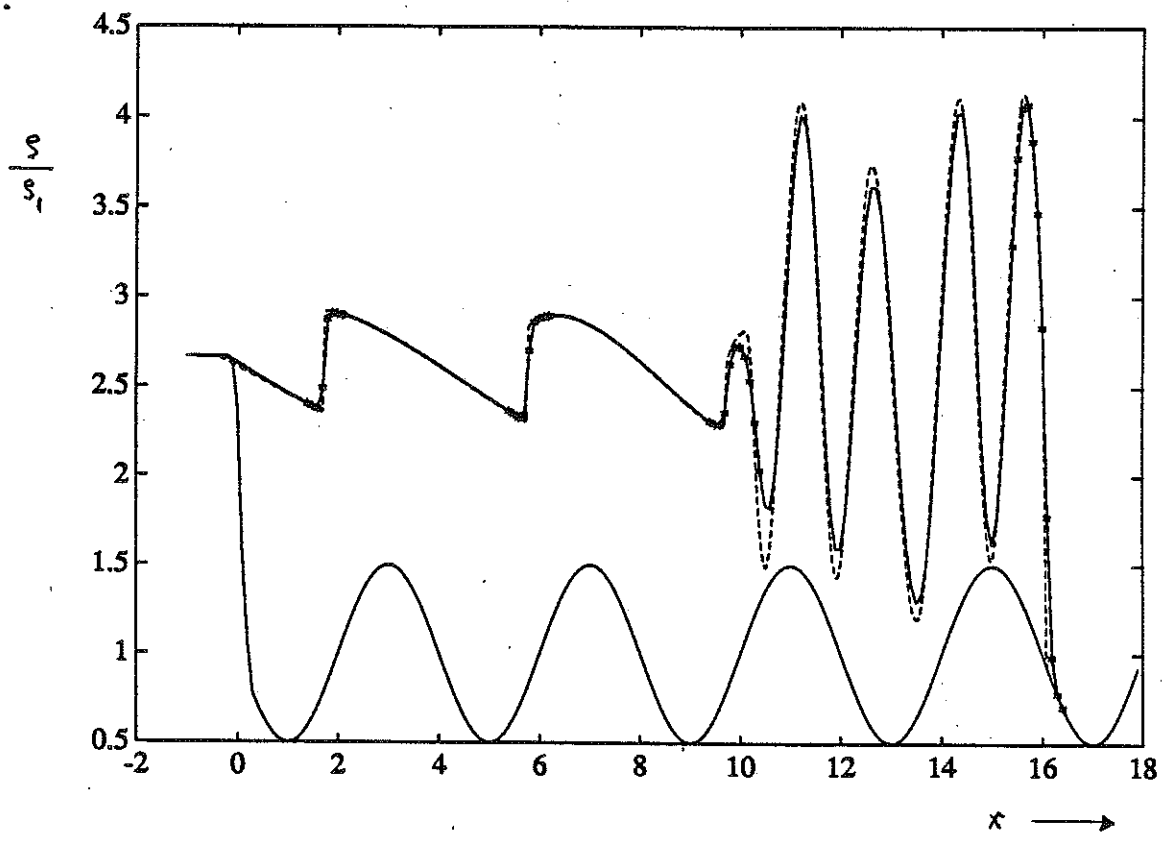

Fig. 11 : Shock / turbulence interaction, $M_{sh} = 2.0$

—×— 3-3 RNDL-ENO, $\Delta x = 0.1$, $\Delta t/\Delta x = 0.25$, ---- exact sol.

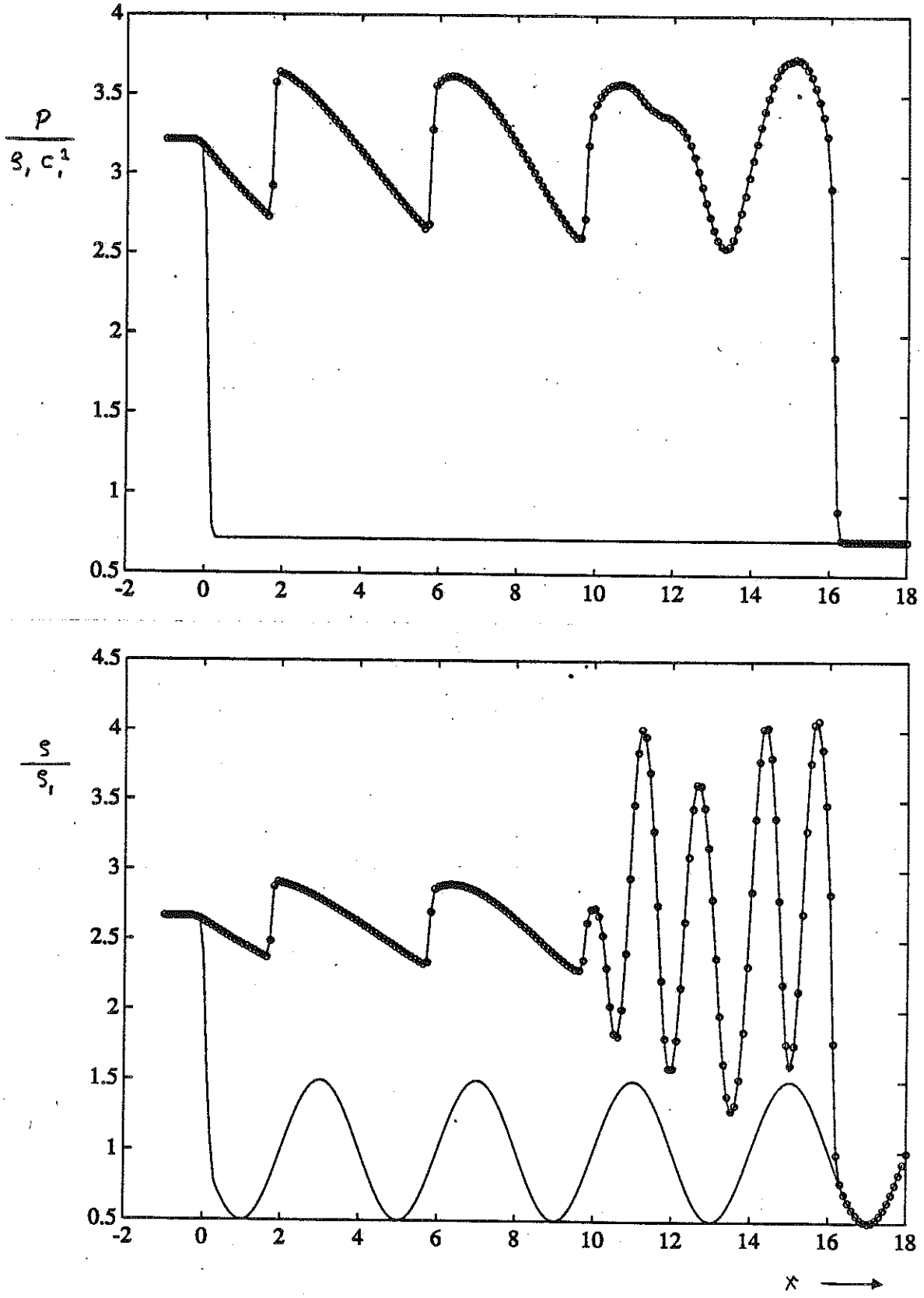

Fig. 12: Shock / turbulence interaction, $M_{sh} = 2.0$

ooooo: RNDL-ENO, ——: NRDL-ENO, $\Delta x = 0.1$, $\Delta t/\Delta x = 0.25$

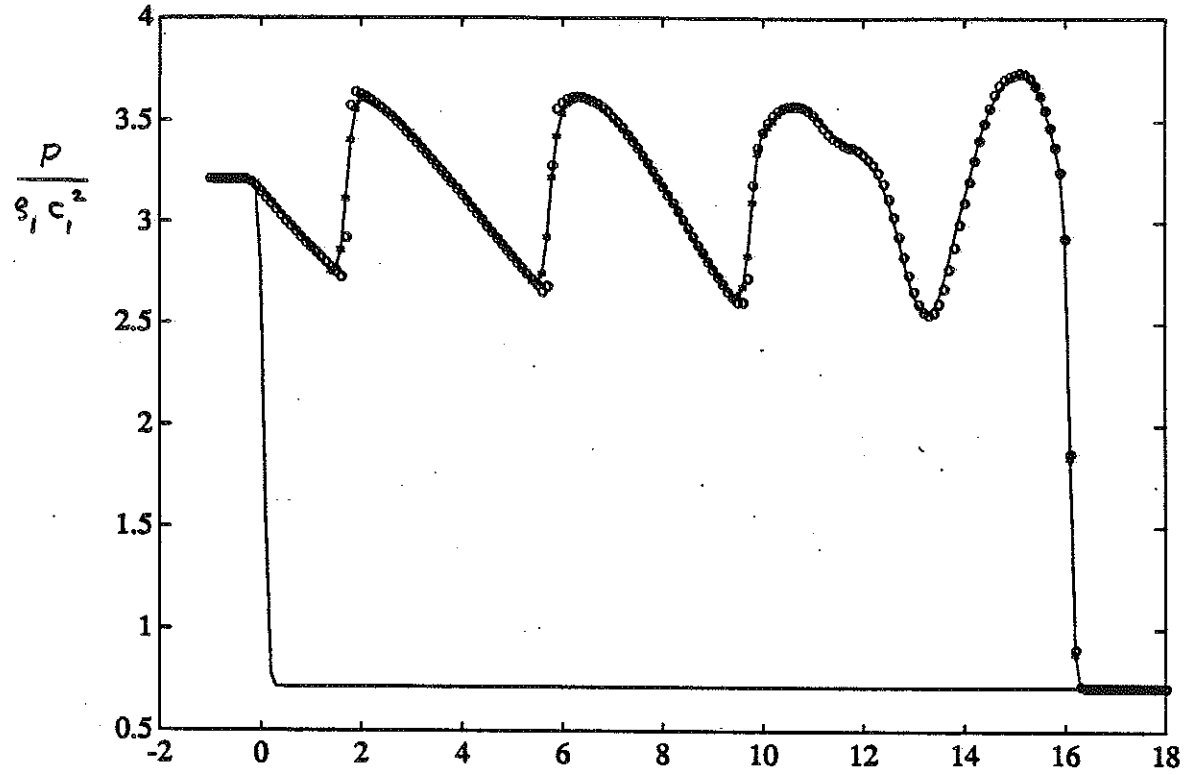

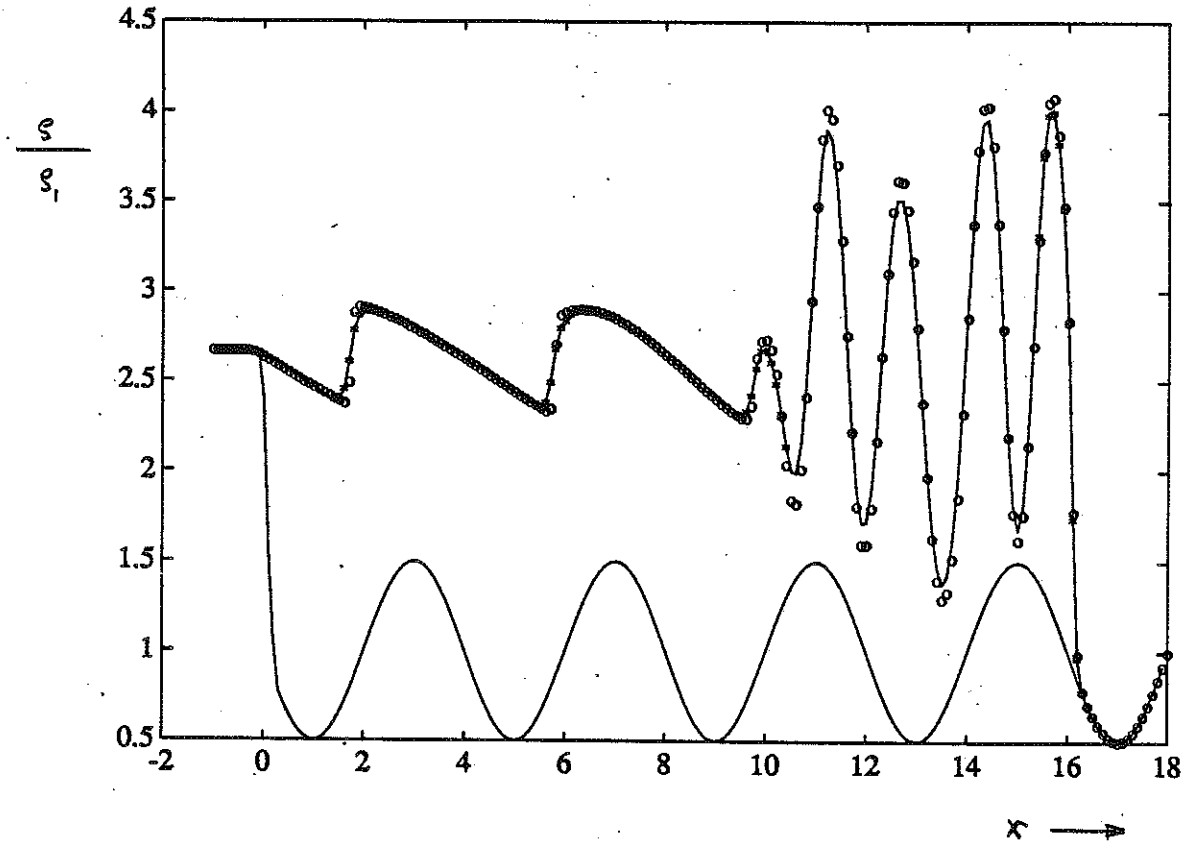

Fig. 13: Shock / turbulence interaction, $M_{sh} = 2.0$

—*— : NDRL ENO, oooo : RNDL-ENO, $\Delta x = 0.1$, $\frac{\Delta t}{\Delta x} = 0.25$

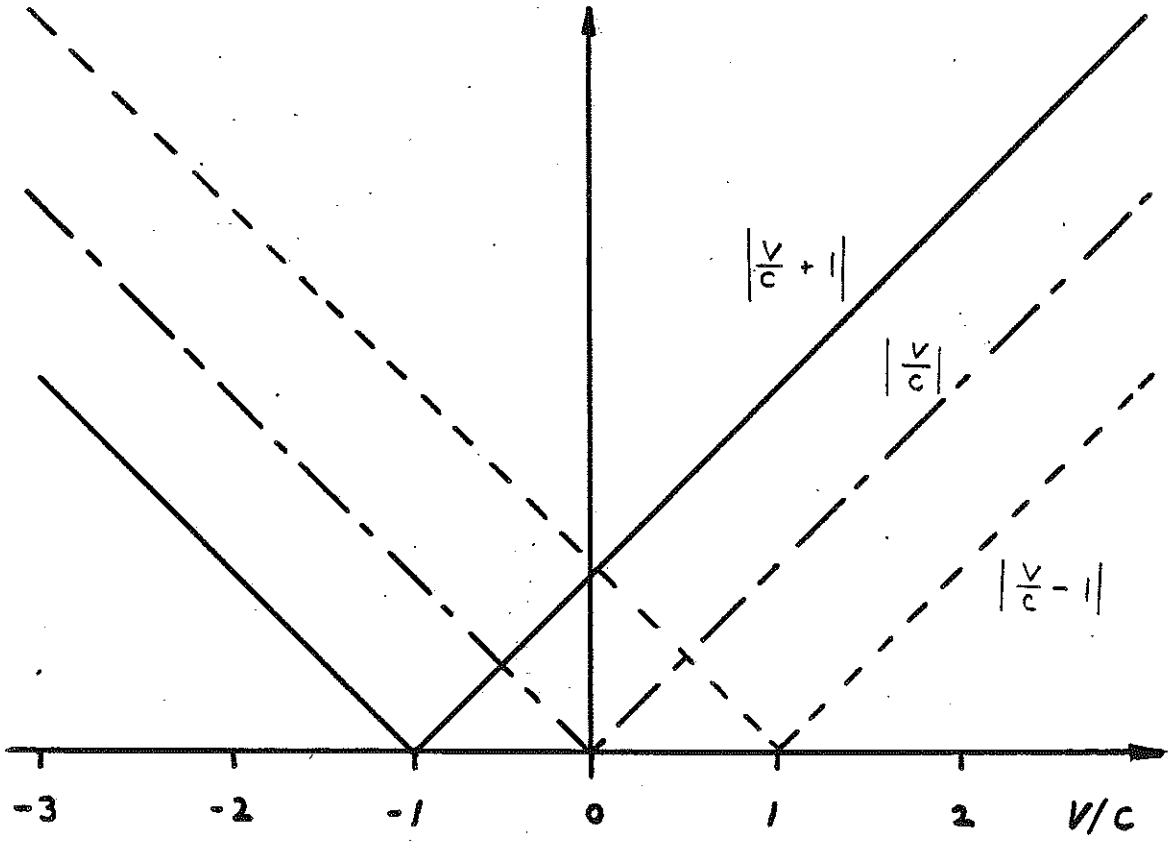

Fig. 14: Absolute values of the eigenvalues of the Jacobian A, one-dimensional gas dynamics.

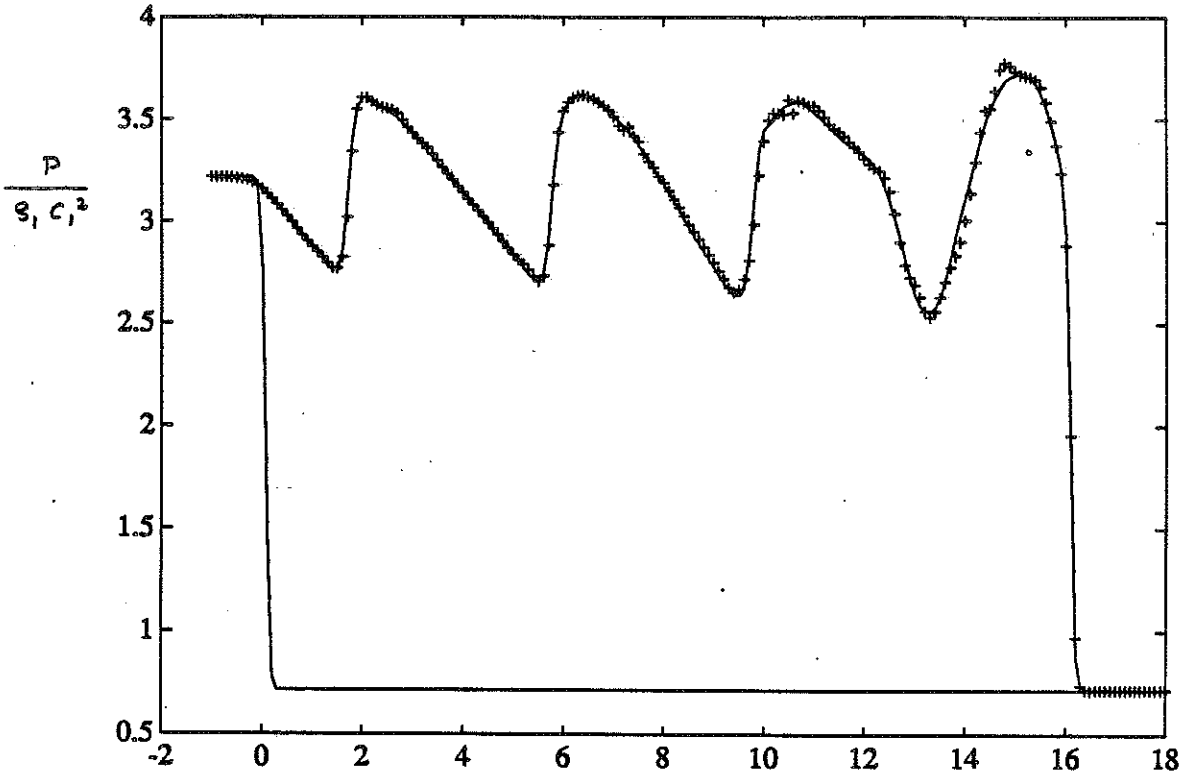

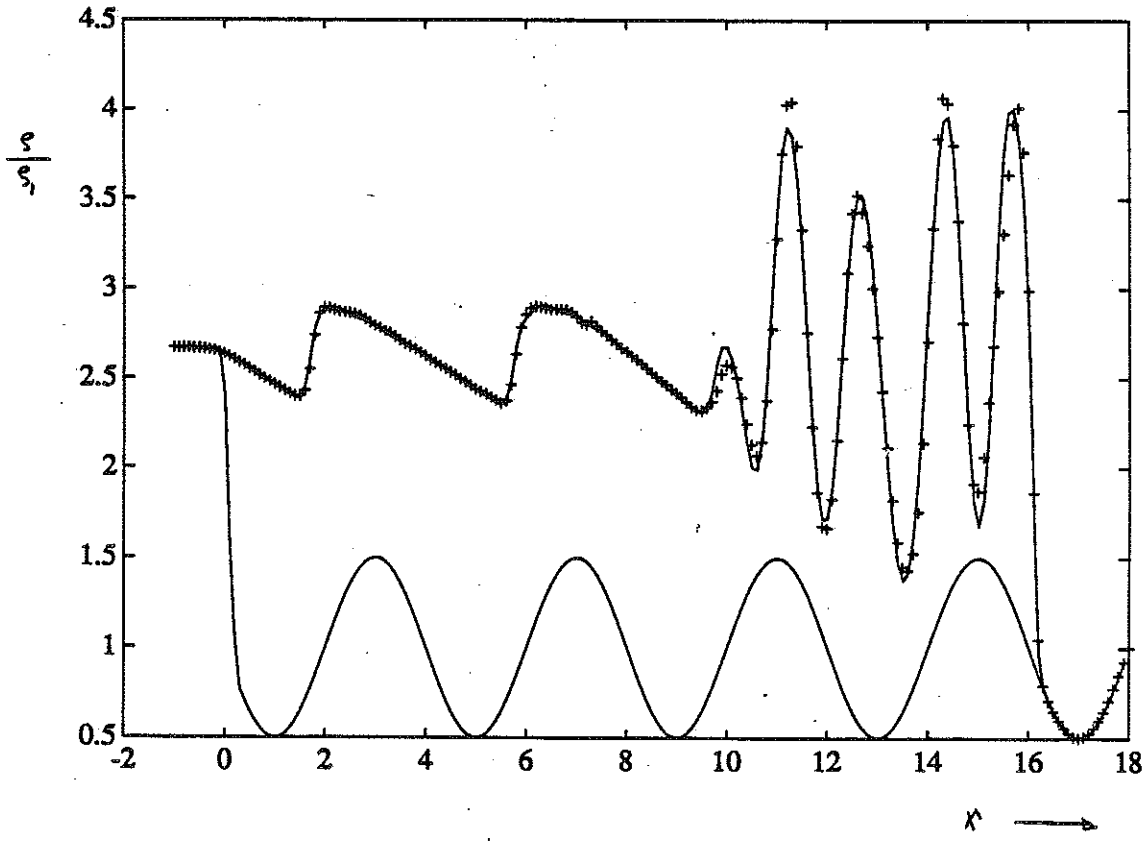

Fig. 15: Shock / turbulence interaction, $M_{sh} = 2.0$

++++ : 3-3 NFU-ENO , ——— : 3-3 NDRL-ENO , $\Delta x = 0.1$, $\Delta t/\Delta x = 0.25$

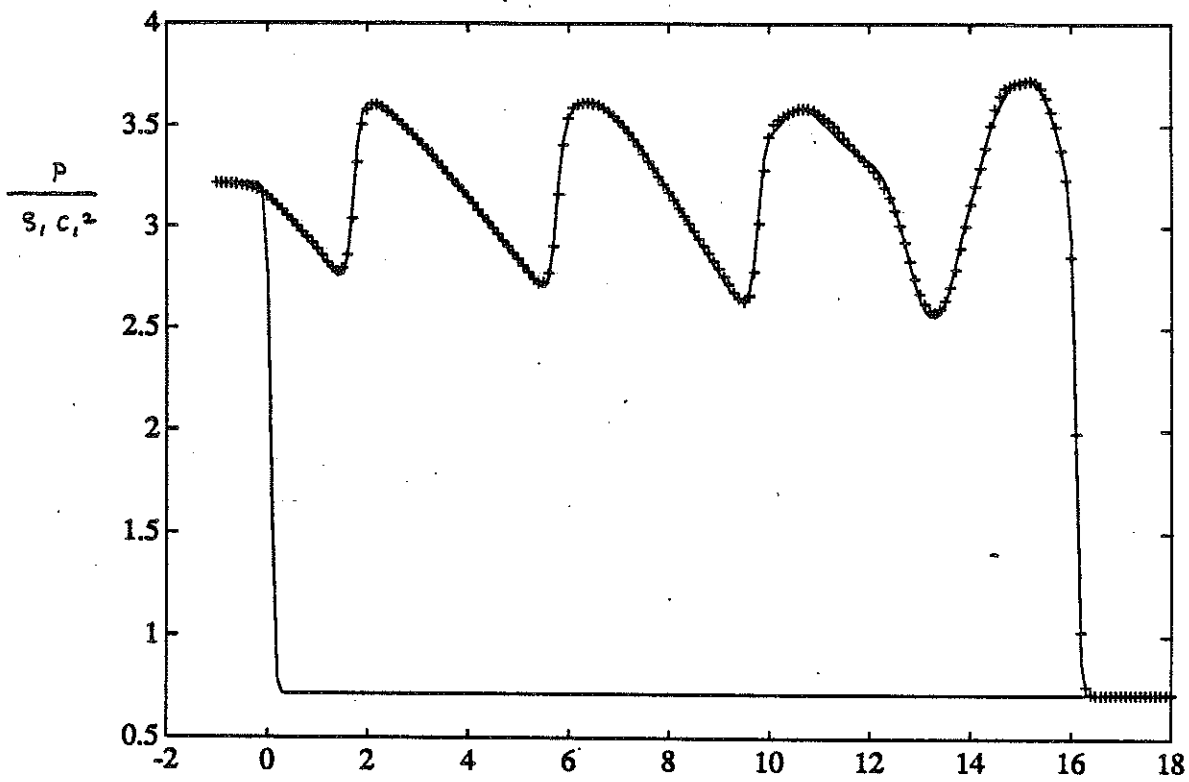

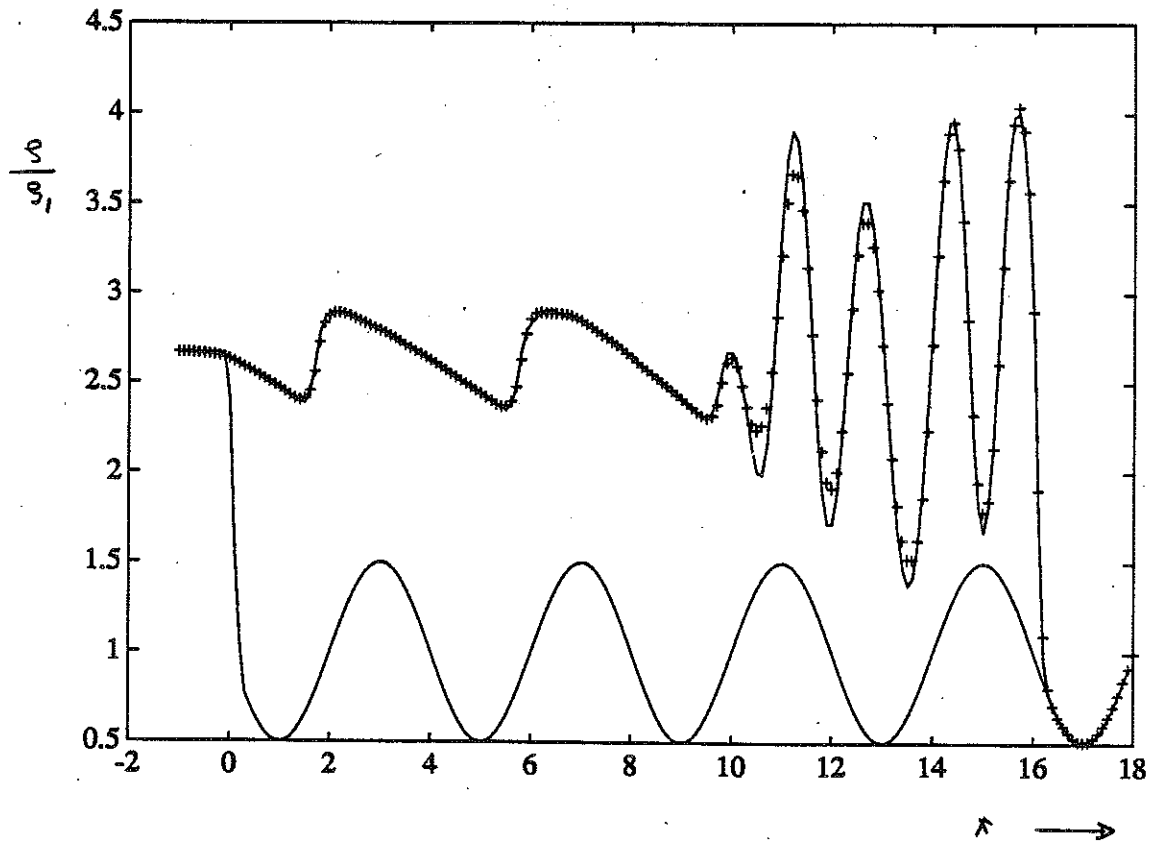

Fig. 16: Shock / turbulence interaction, $M_{sh} = 2.0$

++++ : 2-3 NFU - ENO, ——— : 3-3 NDRL - ENO, $\Delta x = 0.1$, $\frac{\Delta t}{\Delta x} = 0.2$

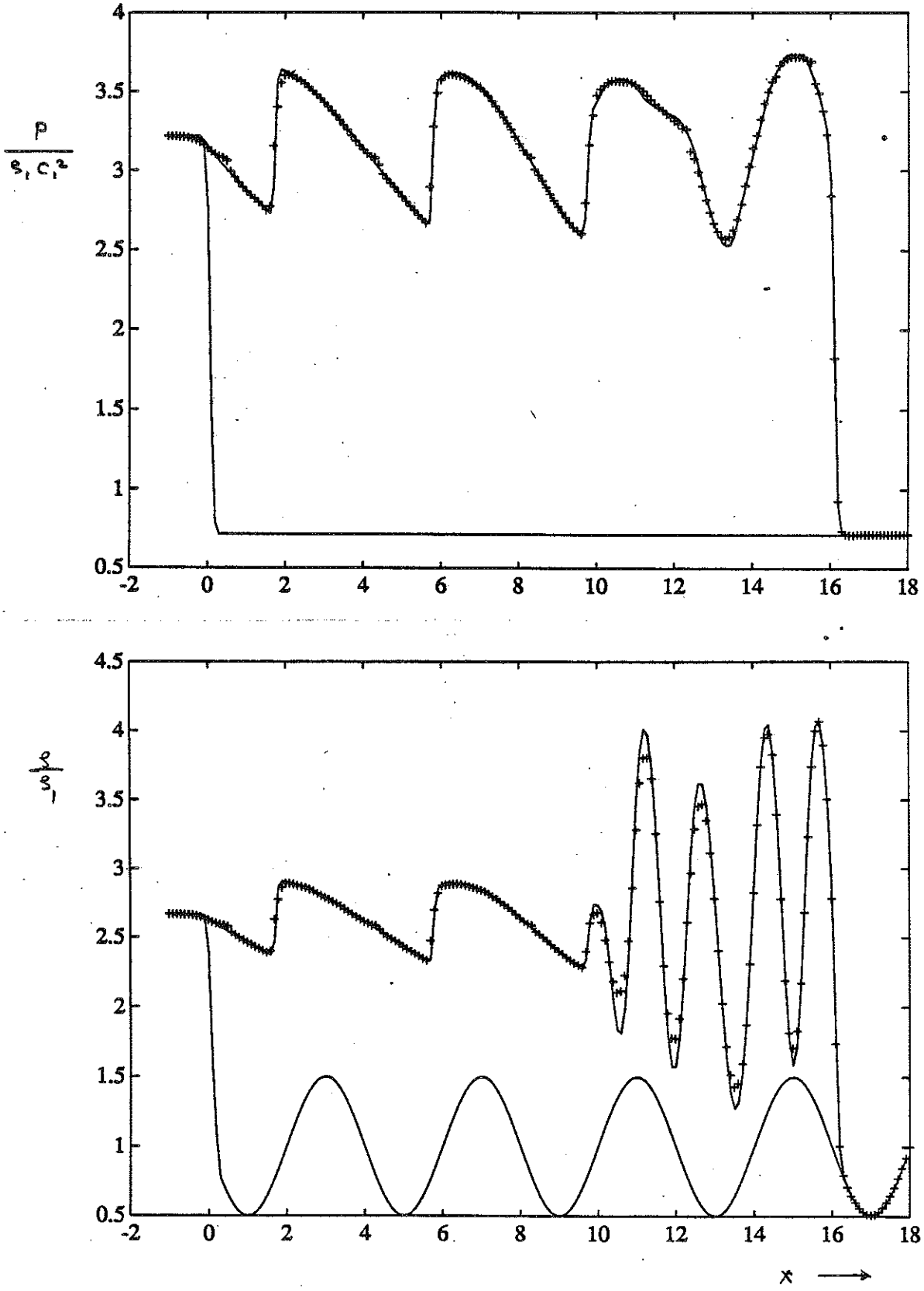

Fig. 17: Shock / turbulence interaction, $M_{sh} = 2.0$

++++ : 2-3 NFA-ENO, ——— : 3-3 NRDL-ENO, $\Delta x = 0.1$, $\Delta t/\Delta x = 0.25$

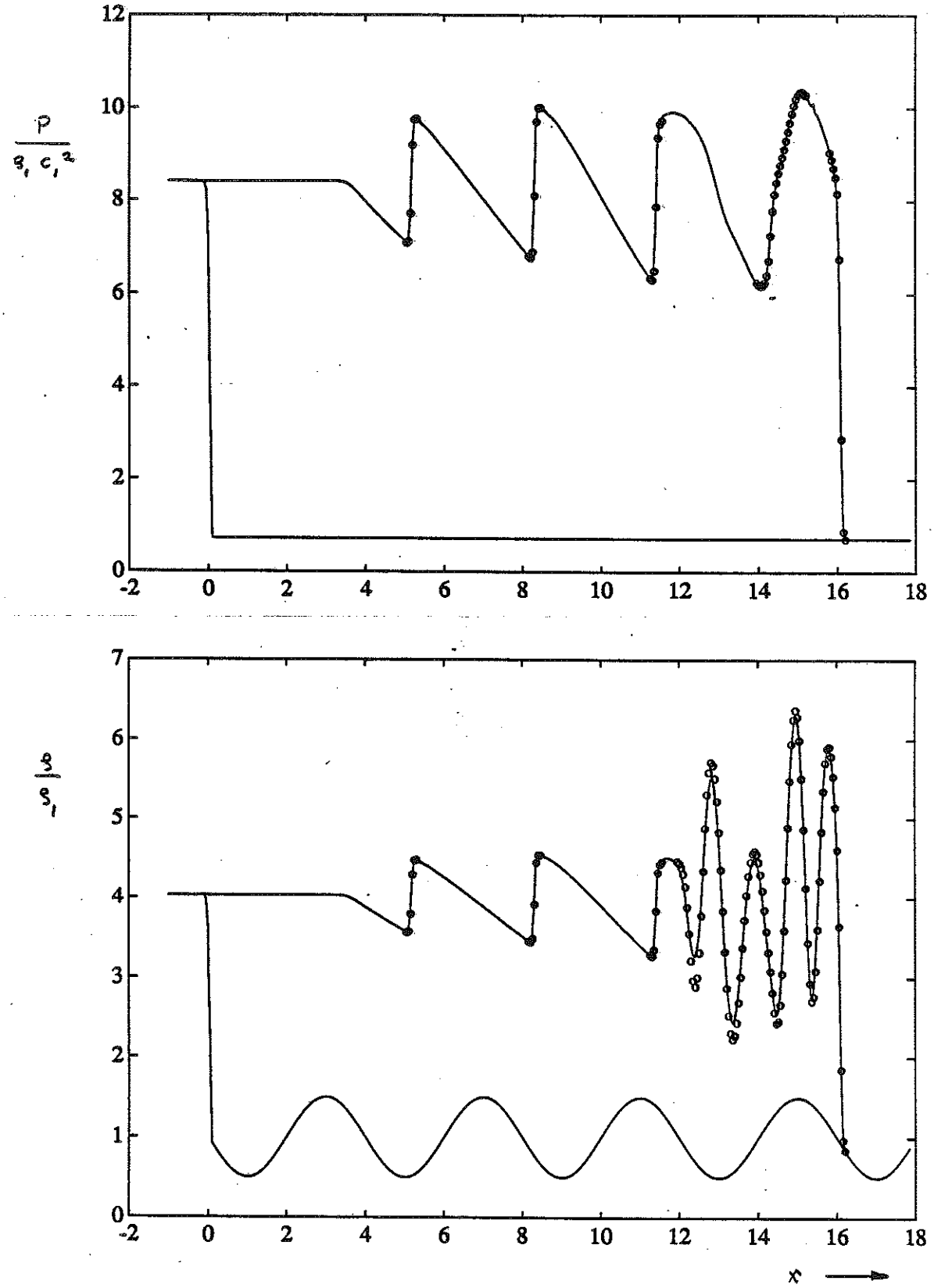

Fig. 18 : Shock / turbulence interaction, $M_{sh} = 3.2$

———— : 2-3 NFA-ENO, oooo : 3-3 RNDL-ENO, $\Delta x = 0.05$, $\frac{\Delta t}{\Delta x} = 0.125$